



## Fixed-point based hierarchical MPC control design for a cryogenic refrigerator<sup>☆</sup>

M. Alamir<sup>a,\*</sup>, P. Bonnay<sup>b</sup>, F. Bonne<sup>b</sup>, V.V. Trinh<sup>a</sup>

<sup>a</sup> CNRS, Univ. Grenoble Alpes, Gipsa-lab, F-3800 Grenoble, France

<sup>b</sup> Univ. Grenoble Alpes, INAC-SBT, F-38000 Grenoble, France



### ARTICLE INFO

#### Article history:

Received 22 March 2017

Received in revised form 3 July 2017

Accepted 5 September 2017

#### Keywords:

Hierarchical MPC

Cryogenic refrigerators

Fixed-point iteration

Modular design

Convergence

Stability

### ABSTRACT

In this paper, a simple, general and scalable hierarchical control framework is proposed and validated through the interconnection of the Joule–Thomson and the Brayton cycle stages of a cryogenic refrigerator. The proposed framework enables to handle the case of destabilizing interconnections through state and/or control signals (which is the case of the cryogenic refrigerator example). Moreover, it offers the possibility to simply change the behavior of the overall system (depending on the context) by only changing the coordinator problem's parameters without changing the set of local controllers used by subsystems which is a common industrial requirement regarding industrial control architectures. Finally, the proposed scheme enables a smooth operator handover on a specific subsystem and/or actuator.

© 2017 Elsevier Ltd. All rights reserved.

## 1. Introduction

Cryogenic refrigerators are used in the experimental facilities containing supra-conducting circuits in order to provide cooling power to cool them down. They are composed of several dozens of subsystems that spread over large areas. Quite often, modifications at some subsystem's level (valve changing and/or control design tuning) frequently take place for many different reasons without appropriate assessment of the impact of such modifications on the overall control design. On the other hand, it is known that cryogenic refrigerators are strongly coupled systems in the sense that fully decentralized solutions cannot be used. The common practice is to tune local controllers (generally PIDs) for the nominal values of the coupling signals and to rely on operator-tuned set-points for these local control-loop during transients and/or severe disturbance modes. Recently, centralized MPC architectures have been proposed [9,6] for the small<sup>1</sup> 400W@1.8 K experimental refrigerator (in

the 400W@4.4 K configuration) at CEA<sup>2</sup>/INAC<sup>3</sup>/SBT<sup>4</sup> [15]. But such a centralized architecture is not an option for real-life cryogenic refrigerators for obvious reasons, among which, the need for each subsystem to send its current state periodically to the coordinator which has also to be aware of any single change in the subsystems hardware/software so that the model of the whole system can be rebuilt and the controller's gains recomputed for all the subsystems.

More generally, it is widely admitted nowadays that non-centralized control architectures are to be preferred, when possible, to fully centralized ones [16,11]. Many reasons for this can be invoked including breaking large problems into small tractable ones, robustness, modularity, privacy preservation and easiness of maintenance.

Non-centralized architectures can be mainly divided into distributed and hierarchical. In the former, no coordinator is used and communication takes place between adjacent neighbors while in the latter, subsystems communicate exclusively with a coordinator which attempts to coordinate the subsystems behavior in order to achieve a global task or to optimize some globally defined performance index.

Excellent reviews of the state of the art regarding these architectures are given in [16,11] as far as Model Predictive Control

<sup>☆</sup> This work has been funded by the French ANR (Agence Nationale pour la recherche) project CRYOGREEN.

\* Corresponding author.

E-mail addresses: [mazen.alamir@gipsa-lab.fr](mailto:mazen.alamir@gipsa-lab.fr) (M. Alamir), [patrick.bonnay@cea.fr](mailto:patrick.bonnay@cea.fr) (P. Bonnay), [francois.bonne@cea.fr](mailto:francois.bonne@cea.fr) (F. Bonne), [vantuong.trinh@gipsa-lab.fr](mailto:vantuong.trinh@gipsa-lab.fr) (V.V. Trinh).

<sup>1</sup> Which spread over two buildings!

<sup>2</sup> Commissariat à l'Energie Atomique.

<sup>3</sup> Institut Nanoscience et Cryogénie

<sup>4</sup> Service des Basses Températures.

(MPC) design is concerned. These reviews show a highly dynamic research area. In particular, the survey book [11] enumerates no less than 35 distinguishable approaches. This makes hard for any new proposed solution to claim full novelty. Instead, let us summarize the items that might help positioning the hierarchical solution proposed in this paper w.r.t existing works on hierarchical control architectures:

✓ Man the optimality and/or constraints fulfillment by assuming the existence of a fully decentralized **stabilizing** feedback [2,8,7]. This strong assumption is not required here nor is it valid for the cryogenic process under interest. On the other hand, our stability result does not theoretically hold in the presence of constraints although it can be technically applied with potential success. This obviously makes the two families of solutions *non comparable* as on one hand, many processes do not fit the fully centralized stabilizability assumption while on the other hand, many processes need constraints to be explicitly handled.

✓ In some works, dedicated assumptions regarding the nature of the coupling signals are introduced in order to avoid strong destabilizing coupling effects. For instance, the framework of [17,12] assumes only coupling through control input actions while in [13] a two layer hierarchical structure is studied where the higher level system is slow with control input given by the lower level. Such assumptions circumvent the major difficulties in strongly coupled systems. In the proposed formulation, strong coupling is allowed (and is shown to be present in the cryogenic example) provided that a controllability assumption is satisfied and an appropriate action is taken by the coordinator in order to stabilize the iterations with the local subsystems. In this contribution, this is done using a fixed-point based iteration.

This paper proposes a first step towards a general, scalable solution to the hierarchical control of cryogenic refrigerators. The solution is described as a *first step* because of the absence of provably-stable constraint handling (although no truly constrained solution is implemented today on a real large cryogenic refrigerators). This drawback is attenuated by the existence of sizing scenarios (worst-case scenarios of interest) that make it possible to assess the feasibility of the unconstrained design on the real system. Note however that this obviously induces a certain amount of conservatism that should obviously motivate a fully constrained hierarchical control assessment as a follow-up of the work proposed in the present paper.

This paper is organized as follows: first of all, the system under study is presented and the control objective is explained in Section 2. This presentation enables the general setting and the proposed solution sketched in Section 3 to be better understood. Section 4 gives the results obtained by means of the proposed hierarchical framework on the cryogenic refrigerator. Finally, Section 5 gives further discussion regarding the proposed solution and how it can be used to smoothly handle the case of operator handover at several levels. Finally, the paper ends by Section 6 which summarizes the paper and gives some hints for further investigations.

## 2. Problem description

### 2.1. Presentation of the cryogenic refrigerator

Cryogenic refrigerators are used in the experimental facilities containing supra-conducting circuits in order to provide cooling power to cool them down. Fig. 1 show the diagram of the 400W@1.8 K experimental refrigerator (in the 400W@4.4 K configuration) at CEA/INAC/SBT [15]. This figure shows also the ideal thermodynamic anti-clockwise cycle in the (entropy–temperature) coordinates.

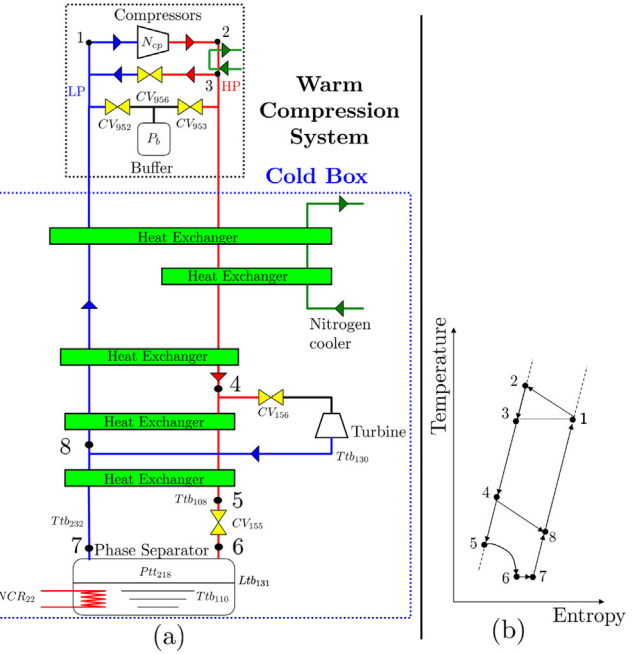


**Fig. 1.** Block diagram of the 400W@1.8 K experimental refrigerator (in the 400W@4.4 K configuration) at CEA/INAC/SBT [15]. (a) The system can be decomposed into two parts: the warm compression system and the cold box. (b) The ideal temperature/entropy diagram.

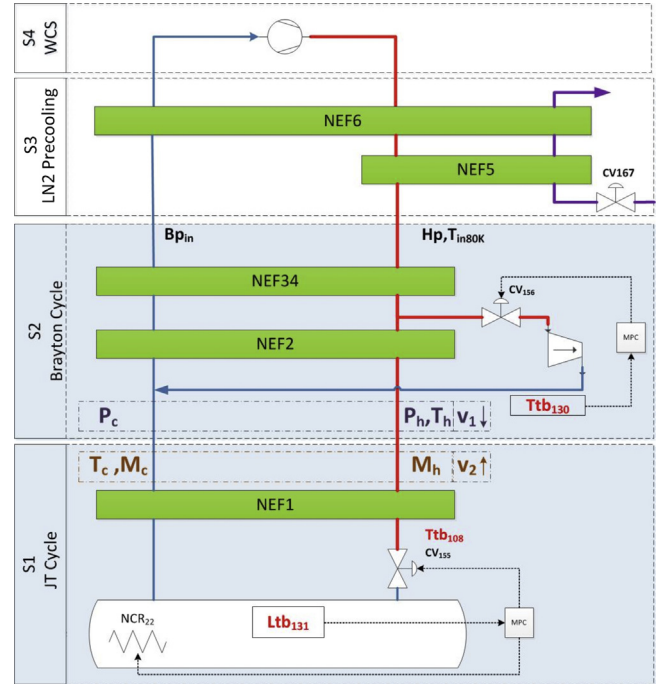


**Fig. 2.** Sketch of the cryogenic refrigerator of CEA-SBT including the two coupled subsystems: S<sub>1</sub>: the Joule–Thomson cycle. S<sub>2</sub>: the Brayton cycle. Fig. 3 shows views of the real system.

Fig. 2 shows the decomposition of the overall process into four interconnected subsystems, in particular, the system to be controlled which is composed of subsystems S<sub>1</sub> (the Joule–Thomson cycle) and S<sub>2</sub> (the Brayton cycle). Generally speaking, a cryogenic refrigerator implements a thermodynamic cycle which produces cooling power by extracting work from a fluid by means of cryogenic turbine (the one following the valve CV<sub>156</sub> in S<sub>2</sub> of Fig. 2) and by exchanging heat power through a series of heat exchangers

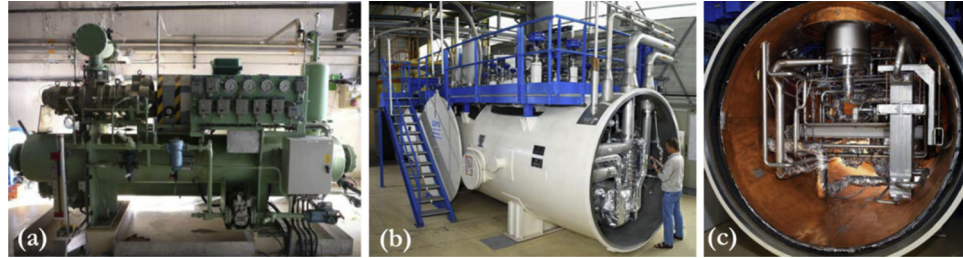


**Fig. 3.** View of the cryogenic plant of CEA-INAC-SBT, Grenoble. (a) The compressor of the warm compression zone (b) Global view of the cold zone (c) details of the cold zone.

(denoted by  $NEF_x$  in Fig. 2). The main objective is to absorb the disturbing heat power generated by the operation of the experimental facility which is represented in the 400 W experimental facility by the heat source denoted by  $NCR_{22}$  in system  $S_1$  of Fig. 2.

Note that in order to close the thermodynamic cycle, a compressor is used in the so-called warm zone (composed of subsystems  $S_3$  and  $S_4$  in Fig. 2) with the objective to maintain pressures (denoted by  $H_p$ ,  $B_p$  in Fig. 2) at some prescribed level which is presumed to be adapted for an optimal behavior of the overall system.

Regarding the dynamic model of the cryogenic refrigerator, a SIMULINK libraries have been developed in [5] in which nonlinear models of all the components (valves, heat exchangers, Helium bath, turbines, compressor) are developed and connected before a linearization is performed around the optimal operation point of the refrigerator. Describing into details this library would obviously go beyond the scope of this contribution, interested reader can refer to [5] and the references therein. As for the state reconstruction and available measurements, the reader can refer to [3] which rigorously discusses the available measurements as well as the way they can be exploited to construct state observers.

In this contribution, it is assumed that the warm zone (systems  $S_3$  and  $S_4$ ) is appropriately controlled (see for instance [4]) and we focus on the control of the so-called cold zone including subsystems  $S_1$  and  $S_2$ . The corresponding control problem is described in the next section. Note that this assumption is quite realistic as the warm zone can be very tightly controlled using the set of valves and the compressor. The satisfaction of this assumption underlined the currently used control design.

## 2.2. The control problem of the cold zone $S_1-S_2$

Using the notation of Fig. 2, the control problem of the cold zone including  $S_1$  and  $S_2$  is described hereafter by successively describing the control inputs, the regulated outputs, the dynamical model and the control objective.

### 2.2.1. The control inputs

There are three control inputs, two of them belong to the Joule–Thomson cycle ( $S_1$ ) and one belongs to the Brayton cycle ( $S_2$ ), more precisely (see Fig. 2):

- (1)  $CV_{155}$ : the position ( $\in [0, 100]$ ) of the valve situated at the input of the Helium bath (Fig. 2). This valve is referred to as the JT-valve.
- (2)  $NCR_{22}^{(a)}$ : the heating power (W) of the resistance inside the helium bath. Recall that this same actuator is used to simulate heat pulses coming from the operation of the physical experimental facility served by the cryogenic refrigerator. This explains the upper index used in  $NCR_{22}^{(a)}$  as the whole power is split into two components  $NCR_{22} = NCR_{22}^{(a)} + NCR_{22}^{(w)}$ , the first of which is used as a control input inside  $S_1$  while the second is used as a disturbance signal. Note that although an observer can be built to estimate the disturbance  $NCR_{22}^{(w)}$  (see [3] for

instance), this disturbance is considered here as an unmeasured disturbance because of the difficulties to predict its future behavior in an MPC design.<sup>5</sup>

- (3)  $CV_{156}$ : the position ( $\in [0, 100]$ ) of the valve situated at the inlet of the cryogenic turbine of  $S_2$ .

### 2.2.2. The regulated outputs

Three output variables need to be regulated, as many as control inputs in each subsystem. More precisely:

- (1)  $Ltb_{131}$ : the level (%) in the liquid helium bath. This variable represents the thermal storage that is immediately available for cooling purposes.
- (2)  $Ttb_{108}$ : the temperature (K) at the inlet of the JT-valve in subsystem  $S_1$  (see Fig. 2). The tight regulation of this variable is crucial in order to maintain the efficiency of the process.
- (3)  $Ttb_{130}$ : the temperature (K) at the outlet of the cryogenic turbine. Maintaining this temperature above a lower limit is mandatory in order to avoid the formation of liquid droplets that can break the turbine.

### 2.3. The nominal operation point

A nominal operation point is defined which is considered to be optimal given the sizing of the refrigerator. This operational point is defined by the stationary values of the inputs, outputs and disturbance described above, namely:

$$CV_{155}^0, NCR_{22}^{(a,0)}, CV_{156}^0, Ltb_{131}^0, Ttb_{108}^0, Ttb_{130}^0 \text{ and } NCR_{22}^{(w,0)} \quad (1)$$

The steady state values are given in Table 1. These values enable the deviations in the inputs, outputs and disturbances to be defined according to:

$$u_1 := \begin{bmatrix} CV_{155} - CV_{155}^0 \\ NCR_{22}^{(a)} - NCR_{22}^{(a,0)} \end{bmatrix}; u_2 := CV_{156} - CV_{156}^0 \quad (2)$$

$$y_1 := \begin{bmatrix} Ltb_{131} - Ltb_{131}^0 \\ Ttb_{108} - Ttb_{108}^0 \end{bmatrix} x; y_2 := Ttb_{130} - Ttb_{130}^0 \quad (3)$$

and

$$w = NCR_{22}^{(w)} - NCR_{22}^{(w,0)} \quad (4)$$

In what follows, the following notation is used to refer to the values at the operation point:

$$U_1^0 := \begin{bmatrix} CV_{155}^0 \\ NCR_{22}^{(a,0)} \end{bmatrix}, U_2^0 := CV_{156}^0, Y_1^0 := \begin{bmatrix} Ltb_{131}^0 \\ Ttb_{108}^0 \end{bmatrix}, Y_2^0 := Ttb_{130}^0 \quad (5)$$

<sup>5</sup> Indeed, the temporal characteristics of the heat pulse depend on the experiment being conducted on the experimental facility. This is required to be unknown by the cryogenic refrigerator.

**Table 1**

Steady state values around which the linear model is computed.

| Variable     | Value | Unit | Variable      | Value | Unit |
|--------------|-------|------|---------------|-------|------|
| $CV_{155}^0$ | 55    | %    | $Ttb_{130}^0$ | 10.41 | K    |
| $CV_{156}^0$ | 50    | %    | $Ttb_{108}^0$ | 5.37  | K    |
| $NCR_{22}^0$ | 407.4 | W    | $Ltb_{108}^0$ | 60.46 | %    |
| $H_p$        | 16    | bar  | $B_p$         | 1.05  | bar  |

One of the main issue regarding the distribution of the optimal nominal operating point  $NCR_{22}^{(0)}$  between  $NCR_{22}^{(a,0)}$  and  $NCR_{22}^{(w,0)}$ , namely:

$$NCR_{22}^{(0)} = NCR_{22}^{(w,0)} + NCR_{22}^{(a,0)} \quad (6)$$

The reason is that for a given value of  $NCR_{22}^{(0)}$ , while the deviation model is the same, higher values of pre-heating power  $NCR_{22}^{(a,0)}$  [and hence lower values of  $NCR_{22}^{(w,0)}$ ] reduce the amount of real heat disturbance power (coming from the operation of the facility the refrigerator is supposed to serve as a cooling source) that is possible to reject. Therefore, the control design should lead to a minimum usage of the control  $NCR_{22}^{(a)}$  in order for lower values of  $NCR_{22}^{(a,0)}$  to be possible to adopt.<sup>6</sup> We will come back to this issue in the simulation section.

### 2.3.1. The dynamic model

Using the index  $s \in \{1, 2\}$  to refer to the subsystem  $S_s$ , the linearized model of the two subsystems, defined around the operating point described above takes the form:

$$x_1^+ = A_1 x_1 + B_1 u_1 + G_1 v_1 + F_1 w_1 \quad (7)$$

$$x_2^+ = A_2 x_2 + B_2 u_2 + G_2 v_2 + F_2 w_2 \quad (8)$$

$$v_1 = C_{v_1} x_2 + D_{v_1} u_2 + E_{v_1} v_2 \quad (9)$$

$$v_2 = C_{v_2} x_1 + D_{v_2} u_1 + E_{v_2} v_1 \quad (10)$$

$$y_1 = C_1 x_1 + D_1 u_1 + E_1 v_1 \quad (11)$$

$$y_2 = C_2 x_2 + D_2 u_2 + E_2 v_2 \quad (12)$$

in which

$\sqrt{x_1 \in \mathbb{R}^{10}}$  and  $x_2 \in \mathbb{R}^{14}$  are the states of subsystems  $S_1$  and  $S_2$  respectively expressed as deviations from the steady state values.

$\sqrt{y_1 \in \mathbb{R}^2}$  and  $y_2 \in \mathbb{R}$  are the deviations of regulated outputs described above.

$\sqrt{v_1 \in \mathbb{R}^3}$  and  $v_2 \in \mathbb{R}^3$  are coupling signals that make the two systems interact dynamically as  $v_1$  depends on  $(x_2, u_2)$  while  $v_2$  depends on  $(x_1, u_1)$ . As a matter of fact  $v_1$  and  $v_2$  both depend on the whole state  $x$  and the control  $u$  as  $v_1$  depends also on  $v_2$  and vice-versa [see (9) and (10)].

More precisely, using the notation of Fig. 2, the coupling variable  $v_1$  is given by

$$v_1 := (P_h, T_h, P_c)^T \in \mathbb{R}^3 \quad (13)$$

where  $P_h$  and  $T_h$  are the pressure and temperature (deviations) at the downstream inlet of the heat exchanger NEF1 while  $P_c$  stands for the pressure (deviation) at the upstream outlet of the same heat exchanger.

Similarly, the coupling variable  $v_2$  is given by:

$$v_2 := (M_h, T_c, M_c)^T \in \mathbb{R}^3 \quad (14)$$

where  $M_h$  is the mass flow rate (deviation) at the downstream inlet of the heat exchanger NEF1 while  $T_c$  and  $M_c$  stand respectively for the temperature and the mass flow rate (deviations) at the upstream outlet of the same heat exchanger.

From these equations, it comes clearly that the two subsystems  $S_1$  and  $S_2$  are strongly coupled since the dynamics of  $S_1$  defined by (7) depends on the variable  $v_1$  which depends through (9) on  $x_2, u_2$ . The same can be said about the dynamics of  $S_2$  which depends on  $S_1$  through the coupling variable  $v_2$  which depends through (10) on  $x_1$  and  $u_1$ .

In the sequel, Eqs. (7)–(12) are sometimes shortly rewritten in the following compact form when linearity is not explicitly involved:

$$x_s^+ = f_s(x_s, u_s, v_s, w_s), s = 1, 2 \quad (15)$$

$$v_1 = g_1(x_2, u_2, v_2) \quad (16)$$

$$v_2 = g_2(x_1, u_1, v_1) \quad (17)$$

$$y_s = h_s(x_s, u_s, v_s, w_s), s = 1, 2 \quad (18)$$

Note that for any initial state  $x(k)$  and any control profile  $u$  defined over some prediction horizon of length  $N$ , the corresponding nominal [disturbance-free] trajectories  $\mathbf{X}(\cdot, u, x(k)|v)$  that are obtained by integrating the dynamics (15)–(17) enable the following so-called coherence constraints to be defined:

$$\mathbf{v}_1(k+i) = g_1(\mathbf{X}_2(k+i, u_2, x_2(k)|v_2), u_2(k+i), v_2(k+i)), \forall i \in \{1, \dots, N\}$$

$$\mathbf{v}_2(k+i) = g_2(\mathbf{X}_1(k+i, u_1, x_1(k)|v_1), u_1(k+i), v_1(k+i)), \forall i \in \{1, \dots, N\}$$

which are obviously two conditions on the coupling variable profiles  $\mathbf{v} := (\mathbf{v}_1, \mathbf{v}_2)$  to be compatible with the system's nominal (disturbance-free) coupled equations. This condition can be shortly written as follows:

$$\mathbf{v}_1 = \mathbf{g}_1(u_2, x_2(k), \mathbf{v}_2) \quad (19)$$

$$\mathbf{v}_2 = \mathbf{g}_2(u_1, x_1(k), \mathbf{v}_1) \quad (20)$$

with obvious appropriate notation. These last conditions are referred to as the **coherence constraints**. In what follows, the obvious notation  $x = (x_1^T, x_2^T)^T$ ,  $y = (y_1^T, y_2^T)^T$ ,  $v = (v_1^T, v_2^T)^T$  are used.

### 2.3.2. The control objective

There are two modes that define the control objective:

- (1) In the first mode which is the by-default mode, the control has to regulate the system  $S_1 \cup S_2$  around  $x=0$  (the nominal steady state operation point invoked above) despite of the presence of non measured disturbance. This is a disturbance rejection mode representing the *raison d'être* of the cryogenic refrigerator.
- (2) In the second mode, the operator should be able to temporary steer the system to a different steady state that corresponds to some new set-point  $y \neq 0$ . For instance, the operator would like to change the level of the liquid helium in the bath (new value of the set-point on  $Ltb_{131}$ ) or on the critical temperature  $Ttb_{108}$ .

These two modes can be accounted for by using different set-points and different weighting matrices in the following *centralized*

<sup>6</sup> Ideally, the heating device  $NCR_{22}$  should not be used as a control variable. But in the current configuration this might lead to feasibility issue in certain cases.

cost function:

$$J_c(\mathbf{u}, x(k)) := \sum_{s=1}^2 \left[ \sum_{i=1}^N \left( \frac{i}{N} \right)^q \left[ \|y_s(k+i) - r_s^d\|_{Q_c^{(s)}}^2 + \|U_s^0 + u_s(k+i)\|_{R_c^{(s)}}^2 \right] \right] \quad (21)$$

where  $\mathbf{u}$  is a candidate sequence of control inputs to be applied starting from the initial state  $x(k)$  over the prediction horizon  $[k, k+N]$ . Note that the output set-points  $r_s^d$ , for  $s=1, 2$  represent the desired values of the deviation on the output corresponding to the set-point  $r_s^d + Y_s^0$ . Finally,  $Q_c^{(1)} \in \mathbb{R}^{2 \times 2}$ ,  $Q_c^{(2)} \in \mathbb{R}_+$ ,  $R_c^{(1)} \in \mathbb{R}^{2 \times 2}$  and  $R_c^{(2)} \in \mathbb{R}^+$  are non-negative weighting matrices.

**Remark 1.** Note that the time-dependent weighting term  $(i/N)^q$  for some  $q \in \mathbb{N}$  enables to put higher weight on the tail of the prediction horizon by taking high value of  $q$ . Note that taking  $q=0$  recover the standard time-invariant stage cost.

**Remark 2.** It is worth underlining that in the cost function (21), the total value of the control inputs is penalized and not the deviation between the input and the steady input that is typically used in a standard Model Predictive Control formulation. This is because in common MPC formulations where the control is penalized through a term of the form  $\|u_s(k+i) - u_s^d\|$ , the stage cost at the desired position is always 0 which obviously does not represent the difference in the real cost that might correspond to each different set-point. Another difference lies in the fact that in order to guarantee the stability of MPC scheme, the whole state should be penalized using a term of the form  $\|x_s(k+i) - x_s^d(r_s^d)\|$  (see [10] for more details). This again leads to a cost function that does not rigorously represent the economic/performance criterion one would intuitively like to minimize. We will see that such formulations which are necessary for the stability of the resulting MPC will be used in the formulation of the local MPC controllers while the realistic and relevant cost function (21) is used to formulate the centralized problem's cost. Such considerations are intimately linked to the concept of economic Model Predictive Control [14] although the latter is generally studied in a non hierarchical framework.

Based on the above definitions and notation, the control problem can be stated as follows:

Define a hierarchical control scheme in which two local MPC controllers, defined for  $S_1$  and  $S_2$  respectively, receive appropriate set-points  $r_1$  and  $r_2$  (send by a coordinator) that minimize the centralized cost function (21) defined for some desired set-point  $r^d$ . Moreover, the following conditions should be satisfied:

### Problem statement

- (1)  $S_1$  and  $S_2$  exclusively communicate with the coordinator
- (2) The coordinator ignores the details of the mathematical models inside  $S_1$  and  $S_2$  and the details of their controllers
- (3) The different modes described above are handled by simply changing the desired set-point  $r^d$  and/or the weighting matrices  $Q_c^{(s)}$  and  $R_c^{(s)}$  of the centralized problem without changing the tuning of the local controllers.

As it is explained later on, there is generally no reason to have  $r=r^d$  as the local costs and the central sub-costs are quite different. The optimal local set-points  $r_s$ ,  $s=1, 2$  are to be computed by the coordinator in order to minimize the central cost corresponding to the original set-point  $r^d$ .

In the next section, a solution is proposed for the above hierarchical control problem in the general case before it is validated on the cryogenic refrigerator in Section 4. It is worth underlying that while the presentation of the next section considers only two subsystems for the sake of clarity and in order to simplify the notation, the framework is obviously applicable almost without change to the case of a networked of several coupled subsystems. Only the notation would be heavier which we prefer to avoid here.

### 3. General setting and proposed solution

In this section, it is first shown (Section 3.1) that a fixed point-like iteration can be defined so that if convergence arises, the coordinator can get a hierarchical estimation of the central cost for a candidate value  $r=(r_1, r_2)$  of the set-points to be sent to the subsystems. For the sake of clarity of exposition, it is first assumed that this convergence occurs systematically and the way the loop is closed to get a hierarchical feedback control addressing the hierarchical control problem stated in the previous section is shown (Section 3.2). The section is then ended by the analysis of the convergence of the fixed point iteration (Section 3.3).

#### 3.1. Hierarchical estimation of the central cost by fixed point negotiation

Let us consider two subsystems  $S_1$  and  $S_2$  which are described by the coupled system of equations given by (15)–(17). Consider also the hierarchical control problem stated at the end of the previous section with the central cost (21). During this subsection, the states  $x_s(k)$ , the central set-point  $r^d$  and the auxiliary individual set-points  $r_s$  are supposed to be given and frozen.

Note first of all that the central optimization problem (21) can be redefined by considering the extended vector of degrees of freedom  $(\mathbf{u}, \mathbf{v})$  as follows:

$$J_c^{ext}(\mathbf{u}, \mathbf{v}, r^d, x(k)) = \sum_{s=1}^2 J_s(\mathbf{u}_s, r_s^d, x_s(k) | \mathbf{v}_s) \quad (22)$$

$$:= \sum_{s=1}^2 \left[ \sum_{i=1}^N \left( \frac{i}{N} \right)^q \left[ \| h_s(k+i) - r_s^d \|_{Q_c^{(s)}}^2 + \| U_s^0 + u_s(k+i) \|_{R_c^{(s)}}^2 \right] \right] \quad (23)$$

where  $h_s(k+.)$  represents the nominal output profile defined by (18):

$$h_s(\sigma) := h_s(\mathbf{X}_s(\sigma, \mathbf{u}_s, x_s(k)|\mathbf{v}_s), \mathbf{u}_s(\sigma), \mathbf{v}_s(\sigma), 0) \quad (24)$$

provided that the coupling signal profiles  $\mathbf{v} = (\mathbf{v}_1, \mathbf{v}_2)$  satisfy the coherence constraints (19) and (20) stated in the previous section:

$$\mathbf{v}_1 = \mathbf{g}_1(\mathbf{u}_2, x_2(k), \mathbf{v}_2) \quad (25)$$

$$\mathbf{v}_2 = \mathbf{g}_2(\mathbf{u}_1, x_1(k), \mathbf{v}_1) \quad (26)$$

Note that in the above cost (22), the two individual costs are now conceptually decoupled for any given choice of the coupling signal profiles  $\mathbf{v}_1$  and  $\mathbf{v}_2$ . The coupling appears now in the coherence equality constraints (25) and (26).

Consequently, the central optimization problem can be rewritten in the following form:

$$\min_{\mathbf{u}_1, \mathbf{u}_2, \mathbf{v}_1, \mathbf{v}_2} \sum_{s=1}^2 J_s(\mathbf{u}_s, r_s^d, x_s(k)|\mathbf{v}_s) \text{ under } \begin{cases} \mathbf{v}_1 = \mathbf{g}_1(\mathbf{u}_2, x_2(k), \mathbf{v}_2) \\ \mathbf{v}_2 = \mathbf{g}_2(\mathbf{u}_1, x_1(k), \mathbf{v}_1) \end{cases} \quad (27)$$

The last form (27) of the central optimization problem is already amenable to hierarchical distribution although it is not the one that will be finally used. Indeed, the coordinator can begin with some initial guesses:

$$\mathbf{v}_1^{(0)}, \mathbf{v}_2^{(0)}$$

of the coupling variables profiles. It sends  $\mathbf{v}_s^{(0)}$  to subsystem  $S_s$ . Each subsystem is now able to compute its own contribution to the central cost, namely:

$$J_s(\mathbf{u}_s, r_s^d, x_s(k)|\mathbf{v}_s^{(0)})$$

for any candidate control profile  $\mathbf{u}_s$ . Therefore, each subsystem can solve its own optimization problem and get its own optimal profile and cost:

$$\mathbf{u}_s^*(r_s^d, x_s(k)|\mathbf{v}_s^{(0)}), J_s^*(r_s^d, x_s(k)|\mathbf{v}_s^{(0)}) \quad (28)$$

Moreover, each subsystem sends what would be the corresponding coupling profile it would apply in this case and **send it to the coordinator**:

$$\text{subsystem } S_1 \text{ send to the coordinator} \rightarrow \hat{\mathbf{v}}_2^{(1)} := \mathbf{g}_2(\mathbf{u}_1^*, x_1(k), \mathbf{v}_1^{(0)}) \quad (29)$$

$$\text{subsystem } S_2 \text{ send to the coordinator} \rightarrow \hat{\mathbf{v}}_1^{(1)} := \mathbf{g}_1(\mathbf{u}_2^*, x_2(k), \mathbf{v}_2^{(0)}) \quad (30)$$

where  $\mathbf{u}_s^* := \mathbf{u}_s^*(r_s^d, x_s(k)|\mathbf{v}_s^{(0)})$ .

Having the new estimations  $\hat{\mathbf{v}}_s^{(1)}$ , the coordinator elaborates a *filtered* version of the coupling profiles:

$$\mathbf{v}_s^{(1)} := (1 - \beta)\mathbf{v}_s^{(0)} + \beta\hat{\mathbf{v}}_s^{(1)} \quad (31)$$

or more generally (see Section 3.3):

$$\mathbf{v}_s^{(1)} := (\mathbb{I} - \Pi_1)\mathbf{v}_s^{(0)} + \Pi_1\hat{\mathbf{v}}_s^{(1)}, \Pi_1 \in \mathbb{R}^{6N \times 6N} \quad (32)$$

and therefore, a fixed-point round of iterations can take place.

The reason why the fixed-point iteration will not be defined as explained above lies in the fact that the centralized cost formulation, when used to built up an MPC feedback design, does not necessarily lead to a stable behavior of the system. Indeed, as it is

noticed earlier, the stability of a finite horizon MPC scheme requires some conditions on the formulation of the cost function (penalizing the whole state, zeros cost at the desired state, positive definite penalty on the control action and so on). Now modifying the central cost in order to meet these requirements may lead to an irrelevant definition from the economic/performance point of view.

Instead, stabilizing formulations are used in the local level in order to enforce stability while only the local set-points  $r_s$  sent by the coordinator to the subsystems are kept as decision variables for the coordinator. This is explained in the remainder of the current section.

More precisely, for each subsystem  $s$ , given a set-point  $r_s$  (not necessarily equal to the central set-point  $r_s^d$ ) together with a current estimation of the coupling profile<sup>7</sup>  $\mathbf{v}_s^{(\sigma)}$ , a local, standard well defined and stability inducing cost function is defined:

$$J_s^{MPC}(\mathbf{u}_s, r_s, x_s(k)|\mathbf{v}_s^{(\sigma)}) := \sum_{i=1}^N \left( \frac{i}{N} \right)^{q_s} \left[ \| x_s(k+i) - x_s^d(r_s) \|_{Q_s}^2 + \| \mathbf{u}_s(k+i) - u_s^d(r_s) \|_{R_s}^2 \right] \quad (33)$$

where

$\sqrt{(x_s^d(r_s), u_s^d(r_s))}$  is the steady pair that is compatible with the output set-point  $r_s$  and the presumed exogenous signal  $\mathbf{v}_s^{(\sigma)}$ .

$\sqrt{x_s(k+i) := \mathbf{X}_s(k+i, \mathbf{u}_s, x_s(k)|\mathbf{v}_s^{(\sigma)})}$  is the nominal predicted state at instant  $k+i$  given the initial state  $x_s(k)$ , the control profile  $\mathbf{u}_s$  and the presumed coupling profile  $\mathbf{v}_s^{(\sigma)}$ .

$\sqrt{q_s}$  is the power used in the time varying penalty that would be necessary to enforce the stability of the local MPC used in subsystem  $s$  following the recent results [1].

The optimal solution of this well-posed optimization problem in the decision variables  $\mathbf{u}_s$  is denoted by

$$\mathbf{u}_s^{opt}(r_s, x_s(k)|\mathbf{v}_s^{(\sigma)})$$

and it is now this sequence that is used to construct the fixed point iteration instead of  $\mathbf{u}^*(r_s^d, x_s(k)|\mathbf{v}_s^{(\sigma)})$  as it is suggested earlier [see (28) and the development that followed].

Therefore, rephrasing (29) and (30) with  $\mathbf{u}_s^{opt}$  instead of  $\mathbf{u}_s^*$  and  $\mathbf{v}_s^{(\sigma)}$  instead of  $\mathbf{v}_s^{(0)}$  leads to:

$$S_1 \text{ send to the coordinator} \rightarrow \hat{\mathbf{v}}_2^{(\sigma+1)} := \mathbf{g}_2(\mathbf{u}_1^{opt}(r_1), x_1(k), \mathbf{v}_1^{(\sigma)}) \quad (34)$$

$$S_2 \text{ send to the coordinator} \rightarrow \hat{\mathbf{v}}_1^{(\sigma+1)} := \mathbf{g}_1(\mathbf{u}_2^{opt}(r_2), x_2(k), \mathbf{v}_2^{(\sigma)}) \quad (35)$$

where  $\mathbf{u}_s^{opt}(r_s) := \mathbf{u}_s^{opt}(r_s, x_s(k)|\mathbf{v}_s^{(\sigma)})$ .

Having the new estimations  $\hat{\mathbf{v}}_s^{(\sigma+1)}$ , the coordinator elaborates a *filtered* version of the coupling profiles:

$$\mathbf{v}_s^{(\sigma+1)} := (1 - \beta)\mathbf{v}_s^{(\sigma)} + \beta\hat{\mathbf{v}}_s^{(\sigma+1)} \quad (36)$$

or more generally (see Section 3.3):

$$\mathbf{v}_s^{(\sigma+1)} := (\mathbb{I} - \Pi_1)\mathbf{v}_s^{(\sigma)} + \Pi_1\hat{\mathbf{v}}_s^{(\sigma+1)}, \Pi_1 \in \mathbb{R}^{6N \times 6N} \quad (37)$$

and therefore, a fixed point-like round of iterations can take place. The whole scheme is sketched in Fig. 4.

Note that in order for the coordinator to compute the estimated value of the central cost function for a given pair  $(r_1, r_2)$  of local set-points, each subsystem evaluates its contribution to the central

<sup>7</sup>  $\sigma=0$  was used in the previous discussion

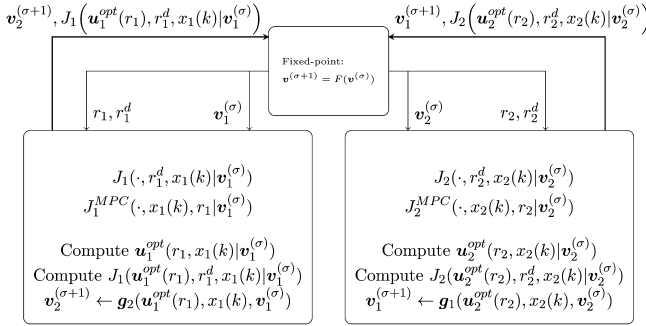


**Fig. 4.** Schematic of the fixed-point iteration that takes place at instant  $k$ , for a frozen states  $x_1(k)$ ,  $x_2(k)$ , and frozen set-points  $r_s$  and  $r_s^d$ .

cost (depending on the central set-points  $r_s^d$ ), **at the optimal profile**  $\mathbf{u}_s^{opt}(r_s)$ , namely:

$$J_s(\mathbf{u}_s^{opt}(r_s), r_s^d, x_s(k)|\mathbf{v}_s^{(\sigma)}) \text{ where } \mathbf{u}_s^{opt}(r_s) := \mathbf{u}_s^{opt}(r_s, x_s(k)|\mathbf{v}_s^{(\sigma)}) \quad (38)$$

and sends it to the coordinator. Upon receiving these evaluations, the coordinator can estimate the value of the central cost for the set-point  $r := (r_1, r_2)$ :

$$J(r|r^d, \mathbf{v}^{(\sigma)}) := \sum_{s=1}^2 \underbrace{J_s(\mathbf{u}_s^{opt}(r_s), r_s^d, x_s(k)|\mathbf{v}_s^{(\sigma)})}_{\text{sent by subsystem } S_s} \quad (39)$$

**Remark 3.** It is important to underline here that the estimation so obtained by the coordinator does not involve the knowledge of the states  $x_s(k)$  nor that of the optimal sequence of control  $\mathbf{u}^{(opt)}$ , these quantity are only known locally in the subsystem which sends the resulting corresponding value of  $J_s$ .

It is important to underline that the above estimation is irrelevant **unless the fixed point iteration converges** toward some fixed point  $\mathbf{v}^{(\infty)}$  since the coherence constraint is not fulfilled otherwise. Said equivalently, if one has:

$$\lim_{\sigma \rightarrow \infty} \mathbf{v}^{(\sigma)} = \mathbf{v}^{(\infty)} \quad (40)$$

then the quadruplet:

$$(\mathbf{u}_1^{opt}(r_1, x_1(k)|\mathbf{v}_1^{(\infty)}), \mathbf{u}_1^{opt}(r_2, x_2(k)|\mathbf{v}_2^{(\infty)}), \mathbf{v}_1^{(\infty)}, \mathbf{v}_2^{(\infty)}) \quad (41)$$

is an admissible<sup>8</sup> sub-optimal solution to the constrained central optimization problem (27). Therefore, only in this case, one can consider that  $J(r|r^d, \mathbf{v}^{(\infty)}(r))$  is the true value of the central cost when the control profiles  $\mathbf{u}_s^{opt}$  are applied by the subsystems.

In order to smoothly introduce the remaining part of the control strategy, the analysis of the conditions under which the above defined fixed-point iteration converges is delayed to Section 3.3. Meanwhile, the next section explains how to built the overall hierarchical feedback in case this convergence unconditionally holds.

### 3.2. Closing the loop

For each value of the auxiliary set-point  $r = (r_1, r_2)$  the coordinator settles the fixed-point round of negotiation with the subsystems, the coordinator obtains after convergence the value of the central cost for this set-point vector  $r \in \mathbb{R}^{n_r}$ , namely

$$J(r|r^d, \mathbf{v}^{(\infty)}(r))$$

which is defined by (39). Now since the above function is quadratic in  $r$ , the coordinator needs to evaluate its value over some grid including more than or equal to  $(n_r + 1)(n_r + 2)/2$  different nodes in order to reconstruct the central cost as a quadratic function of  $r$ , namely:

$$\hat{J}(r) = \frac{1}{2} r^T Q r + f^T r + c \quad (42)$$

where  $Q \in \mathbb{R}^{n_r \times n_r}$ ,  $f \in \mathbb{R}^{n_r}$  and  $c \in \mathbb{R}$  depends obviously on  $r^d$  and  $x(k)$  in a way that is analytically unknown to the coordinator.

This can obviously be done by taking a regular grid around  $r^d$  such as the one defined by:

$$r_i^{(j)} := r_i^d + g_i^{(j)} \cdot \Delta, (i, j) \in \{1, \dots, n_r\} \times \{1, \dots, m^{n_r}\} \quad (43)$$

$$g^{(j)} \in [\mathcal{N}_m]^{n_r}, N_m := \{-1, \dots, +1\} \in \mathbb{R}^{n_r} \quad (44)$$

for some  $\Delta > 0$  and some integer  $m$  such that  $m^{n_r} \geq (n_r + 1)(n_r + 2)/2$ . The coefficients  $Q$ ,  $f$  and  $c$  of the quadratic form can therefore be computed by solving the least squares problem:

$$(\text{Coordinator}) \min_{Q, f, c} \sum_{j=1}^{m^{n_r}} \left| \hat{J}(r^{(j)}) - \left[ \frac{1}{2} \|r^{(j)}\|_Q^2 + f^T r^{(j)} + c \right] \right|^2 \quad (45)$$

Once  $Q, f$  are available, the optimal auxiliary set-point can be computed according to:

$$r^{opt}(k) := -Q^{-1}f \quad (46)$$

This optimal set-point is therefore sent to the subsystems with an *end-of-iterations* flag which is interpreted by the subsystem as the definitive optimal set-point at instant  $k$ . Based on this information and in accordance with the receding-horizon principle, the first action in the corresponding optimal sequences, namely

$$u_s(k) := [\mathbb{I}_{n_s^u}, \mathbb{O}_{n_s^u}, \dots, \mathbb{O}_{n_s^u}] \mathbf{u}_s^{opt}(r_s^{opt}(k), x_s(k)|\mathbf{v}_s^{(\infty)}) \quad (47)$$

is applied by subsystem  $S_s$  during the sampling period  $[k, k+1]$ .

Note that this implicitly assumes that the computation time for the  $m^{n_r}$  iterations is negligible when compared to the sampling period of the control loop. This is not a strong assumption as the computation at each iteration is given by the matrix multiplication as it is shown in the next section. Note also that the scheme should include an anticipative action in the sense that the computation of  $u_s(k)$  should be done during the previous sampling period  $[k-1, k]$  based on each subsystem estimation of its future state at instant  $k$ . These are standard implementation tricks that have been skipped here in order to focus on the main message.

This completely defines the hierarchical control algorithm. In the next section, the analysis of the convergence of the fixed point iteration is done.

### 3.3. Convergence of the fixed-point iteration

In order to analyze the convergence of the fixed point iteration, we begin by establishing the dynamics that governs the successive iterates  $\mathbf{v}^{(\sigma)}$ . To do this, note that at each iteration, subsystem  $S_s$  solves a finite horizon unconstrained quadratic optimization problem in which the only exogenous information is represented by the current state  $x_s(k)$ , the auxiliary set-point  $r_s$  and the exogenous coupling signal  $\mathbf{v}_s^{(\sigma)}$ , therefore, the optimal control profile  $\mathbf{u}_s^{opt}$  computed by subsystem  $S_s$  takes the following form:

$$\mathbf{u}_1^{opt} := [K_1^{(x)}]x_1(k) + [K_1^{(r)}]r_1 + [K_1^{(v)}]\mathbf{v}_1^{(\sigma)} \quad (48)$$

$$\mathbf{u}_2^{opt} := [K_2^{(x)}]x_2(k) + [K_2^{(r)}]r_2 + [K_2^{(v)}]\mathbf{v}_2^{(\sigma)} \quad (49)$$

with straightforward definition of the gain matrices.

On the other hand, the updated value  $\hat{\mathbf{v}}_1^{(\sigma+1)}$  [resp.  $\hat{\mathbf{v}}_2^{(\sigma+1)}$ ] is nothing but output of a linear system with initial state  $x_1(k)$  [resp.  $x_2(k)$ ],

<sup>8</sup> In the sense of the satisfaction of coherence constraints (19) and (20).

---

**Algorithm 1** Fixed-point iteration to evaluate  $J(r \mid r^d, \mathbf{v}^{(\infty)}(r))$ 


---

- 1: **local data at subsystems:**  $x_1(k), x_2(k)$
- 2: **shared data between Coordinator and  $S_s$ :** set-points  $r_s^d, r_s, \bar{M}_s^{(v)}$
- 3: **data available to the coordinator.**  $\bar{M}^{(v)}$  [see (53)],  $\Pi_1$  (using dlqr)
- 4: **Initialization.**  $\sigma = 0, \mathbf{v}_s^{(0)} = 0, s = 1, 2, \delta^{(0)} = 1$
- 5: **while**  $\delta^{(\sigma)} > \varepsilon$  **do**
- 6:   Coordinator sends  $\mathbf{v}_s^{(\sigma)}$  to  $S_s, s = 1, 2$
- 7:   Subsystem  $S_s$  computes  $\mathbf{v}_s^{(\sigma+1)}$  according to (48)–(51)
- 8:   Subsystem  $S_s$  sends  $\mathbf{v}_s^{(\sigma+1)}$  to the coordinator
- 9:   Coordinator computes  $\mathbf{v}_s^{(\sigma+1)}, s = 1, 2$  using (59)
- 10:   Coordinator computes  $\delta^{(\sigma+1)} \leftarrow \|\mathbf{v}^{(\sigma+1)} - \mathbf{v}^{(\sigma)}\|$
- 11:    $\sigma \leftarrow \sigma + 1$
- 12: **end while**
- 13: Coordinator sets  $\mathbf{v}_s^{(\infty)} \leftarrow \mathbf{v}_s^{(\sigma+1)}, s = 1, 2$
- 14: Coordinator sends  $\mathbf{v}_s^{(\infty)}$  to  $S_s$  with end-of-iteration flag
- 15: Subsystem  $S_s$  compute the optimal control  $\mathbf{u}_s^{opt}(r_s, x_s(k) | \mathbf{v}_s^{(\sigma)})$
- 16: Subsystem  $S_s$  computes  $J_s(\mathbf{u}_s^{opt}, r_s^d, x_s(k) | \mathbf{v}_s^{(\infty)})$  involved in (22) and sends it to the coordinator
- 17: Coordinator compute the cost

$$J(r | r^d, \mathbf{v}^{(\infty)}) := \sum_{s \in \{1, 2\}} J_s(\mathbf{u}_s^{opt}, r_s^d, x_s(k) | \mathbf{v}_s^{(\infty)})$$

- 18: End of the fixed-point iteration round.
- 

**Fig. 5.** Summary of the fixed-point iteration between the coordinator and the subsystems in order to compute the central cost for a given pair of set-point  $r_s, s = 1, 2$ .

input profiles given by (48) [resp. (49)] and affected by coupling signal  $\mathbf{v}_1^{(\sigma)}$  [resp.  $\mathbf{v}_2^{(\sigma)}$ ]. This can be written as follows:

$$\hat{\mathbf{v}}_1^{(\sigma+1)} := [M_2^{(x)}] x_2(k) + [M_2^{(u)}] \mathbf{u}_2^{opt} + [M_2^{(v)}] \mathbf{v}_2^{(\sigma)} \quad (50)$$

$$\hat{\mathbf{v}}_2^{(\sigma+1)} := [M_1^{(x)}] x_1(k) + [M_1^{(u)}] \mathbf{u}_1^{opt} + [M_1^{(v)}] \mathbf{v}_1^{(\sigma)} \quad (51)$$

with straightforward definition of the gain matrices. Combining (48)–(51) obviously leads to:

$$\hat{\mathbf{v}}^{(\sigma+1)} = [\bar{M}^{(v)}] \mathbf{v}^{(\sigma)} + [\bar{M}^{(r)}] r + [\bar{M}^{(x)}] x(k) \quad (52)$$

where

$$[\bar{M}^{(v)}] := \begin{bmatrix} \mathbb{O} & M_2^{(v)} + M_2^{(u)} K_2^{(v)} \\ M_1^{(v)} + M_1^{(u)} K_1^{(v)} & \mathbb{O} \end{bmatrix} =: \begin{bmatrix} \mathbb{O} & \bar{M}_2^{(v)} \\ \bar{M}_1^{(v)} & \mathbb{O} \end{bmatrix} \quad (53)$$

$$[\bar{M}^{(r)}] := \begin{bmatrix} \mathbb{O} & M_2^{(r)} + M_2^{(u)} K_2^{(r)} \\ M_1^{(r)} + M_1^{(u)} K_1^{(r)} & \mathbb{O} \end{bmatrix} \quad (54)$$

$$[\bar{M}^{(x)}] := \begin{bmatrix} \mathbb{O} & M_2^{(x)} + M_2^{(u)} K_2^{(x)} \\ M_1^{(x)} + M_1^{(u)} K_1^{(x)} & \mathbb{O} \end{bmatrix} \quad (55)$$

and finally, using (52) in the updating rule (36) one obtains the dynamics that governs the fixed point iteration:

$$\mathbf{v}^{(\sigma+1)} = \underbrace{[(1 - \beta)\mathbb{I} + \beta \bar{M}^{(v)}]}_{Z(\beta)} \mathbf{v}^{(\sigma)} + \beta [[\bar{M}^{(r)}] r + [\bar{M}^{(x)}] x(k)] \quad (56)$$

This clearly indicates that the convergence of the fixed-point iteration is conditioned by the spectrum radius of the matrix  $Z(\beta)$  defined above. More precisely:

$$\{\text{The fixed-point iteration converges}\} \Leftrightarrow \{\rho(Z(\beta)) < 1\} \quad (57)$$

where  $\rho(Z)$  is the spectrum radius of the matrix:

$$\rho(Z(\beta)) := \max_i |\lambda_i(Z(\beta))| \quad (58)$$

The filtering law (36) is obviously over simplified. More elaborated filters can be used in case the simple rule does not allow convergence for any possible value of  $\beta \in (0, 1)$ . More precisely, one can seek a filtering rule of the form:

$$\mathbf{v}^{(\sigma+1)} = (\mathbb{I} - \Pi_1) \mathbf{v}^{(\sigma)} + \Pi_1 \hat{\mathbf{v}}^{(\sigma+1)} \quad (59)$$

which leads to a convergent fixed-point iteration provided that the following condition holds [by virtue of (52)]:

$$\rho(\mathbb{I} - \Pi_1 + \Pi_1 \bar{M}^{(v)}) < 1 \quad (60)$$

which can always be satisfied for a convenient  $\Pi_1$  provided that:

$$\text{The pair } (\mathbb{I}, [I - \bar{M}^{(v)}]^T) \text{ is controllable} \quad (61)$$

Indeed, if this is the case, the spectrum radius (60) can be assigned using standard design tool such as the subroutine DLQR of MATLAB. Moreover, the spectrum can theoretically made as small as necessary to force the convergence in a few number of iterations.

The above arguments enable to state the following result:

**Fixed-point convergence certification**

The matrices  $\{\bar{M}_s^{(v)}\}_{s \in \{1, 2\}}$  summarize the static information the coordinator needs to have in order to be able to check and to certify the convergence (if any) of the fixed-point iteration that is in the heart of the proposed hierarchical framework. Having these

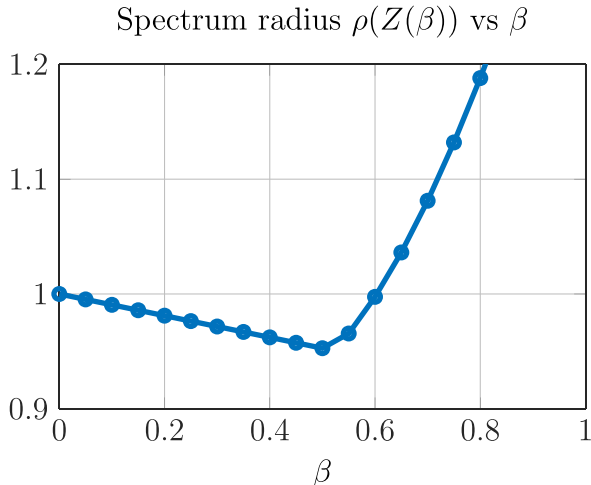


**Fig. 6.** Evolution of the spectrum radius of the matrix  $Z(\beta)$  [see (56)] governing the stability of the fixed point iteration as a function of the filtering coefficient  $\beta$ .

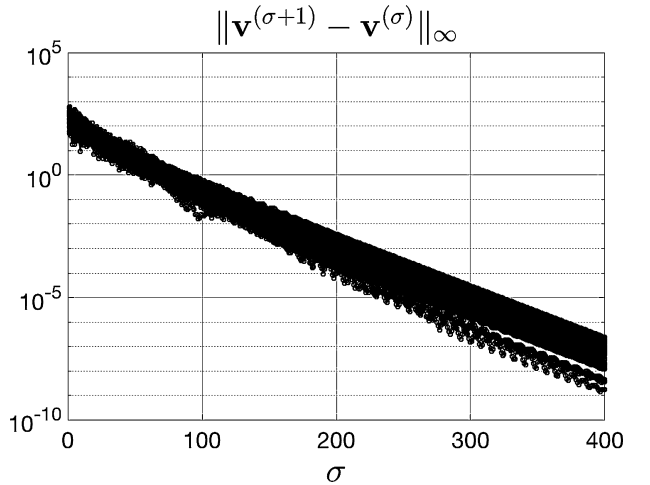


**Fig. 7.** Evolution of the maximum error between two successive coupling signal during the fixed point iterations. 50 random initial values  $\mathbf{v}^{(0)}$  are simulated.

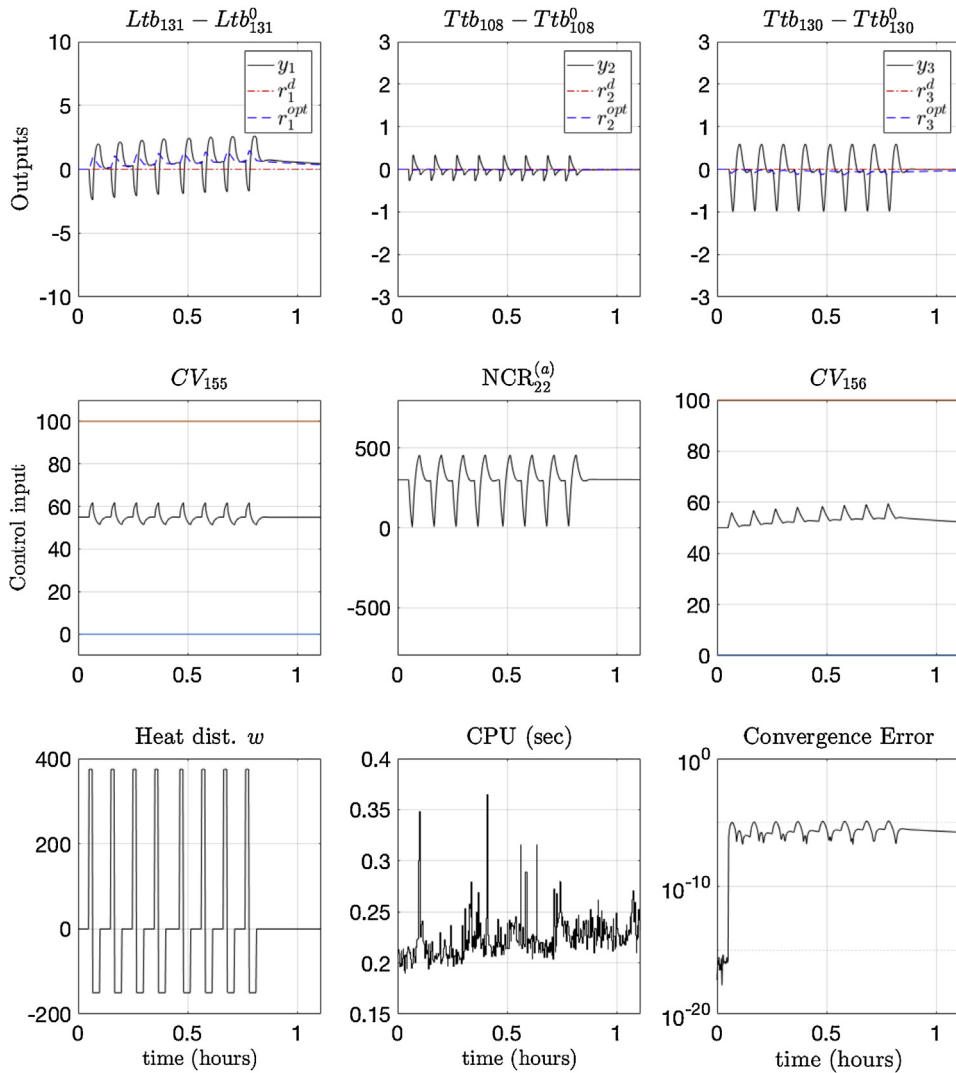


**Fig. 8.** Behavior of the closed-loop process under heat pulse disturbance.

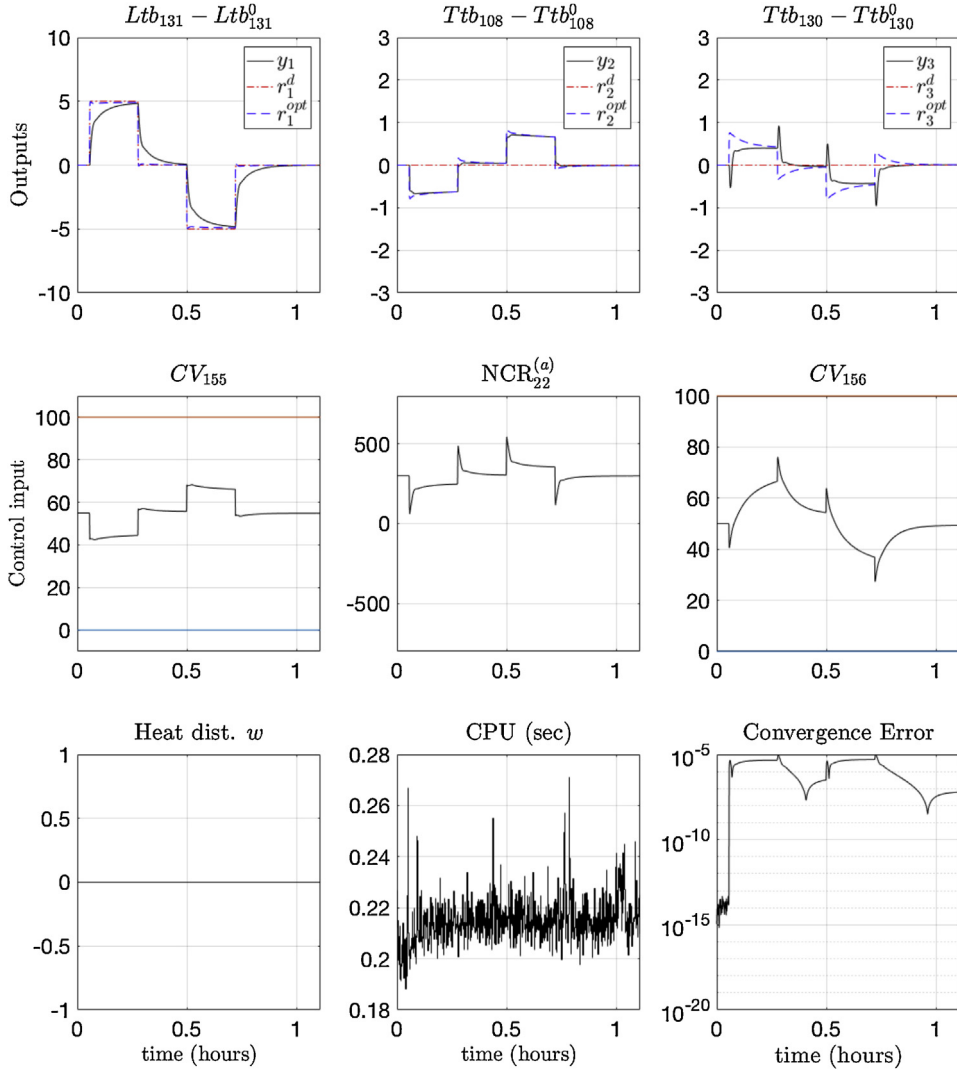


**Fig. 9.** Behavior of the closed-loop process in mode 2 in which the regulation of liquid level  $Ltb_{131}$  is privileged. Note how the regulation of the temperature  $Ttb_{108}$  is softened in order to perform the required task on the regulated level. (For interpretation of the references to color in the text, the reader is referred to the web version of the article.)

matrices, the coordinator might appropriately choose the filtering parameter in order guarantee the convergence.

**Remark 4.** Note that the matrices  $\bar{M}_s^{(v)}$  represent a high level condensed information that does not depend on the state of subsystem  $S_s$ , neither it depends on the number of actuators or the precise control law settings that are used in the local level.

At this point it is possible to summarize the steps leading to the evaluation of  $J(r|r^d, \mathbf{v}^{(\infty)}(r))$  in Algorithm 1 depicted in Fig. 5.

In the validation section, both filtering rules are shown over a set of validating scenarios.

#### 4. Simulation results

In this section, the hierarchical MPC framework proposed in the previous section is applied to address the hierarchical control problem of the cryogenic refrigerator. More precisely, two validation sets are shown in order to strengthen the relevance of the two non-conventional aspects of the design namely:

- (1) The use of time varying weighting cost in (33) in the definition of the local MPC design.

- (2) The use of spectrum assignment through LQR (Linear Quadratic Regularizer) based design in order to guarantee the convergence of the fixed point iteration as discussed in the end of the previous section.

In particular, it will be shown that without these two new features, although the problem can be solved, the results are not totally satisfactory because of the excessive use of the control actuator  $NCR_{22}^a$  which implies a high value of steady heat value and therefore a drop in the energy efficiency of the refrigerator. It is then shown that the use of the above two features enables a better use of the refrigerator and to a complete solution of the problem being addressed.

##### 4.1. Results with standard design of local MPC and simple filtering rule

The following validation topics are successively addressed.

- (1) First of all, the convergence of the fixed-point iteration is analyzed for different values of the filtering parameter  $\beta$ .
- (2) Then the by-default regulation scenario is simulated and the performance of the closed-loop system is shown.

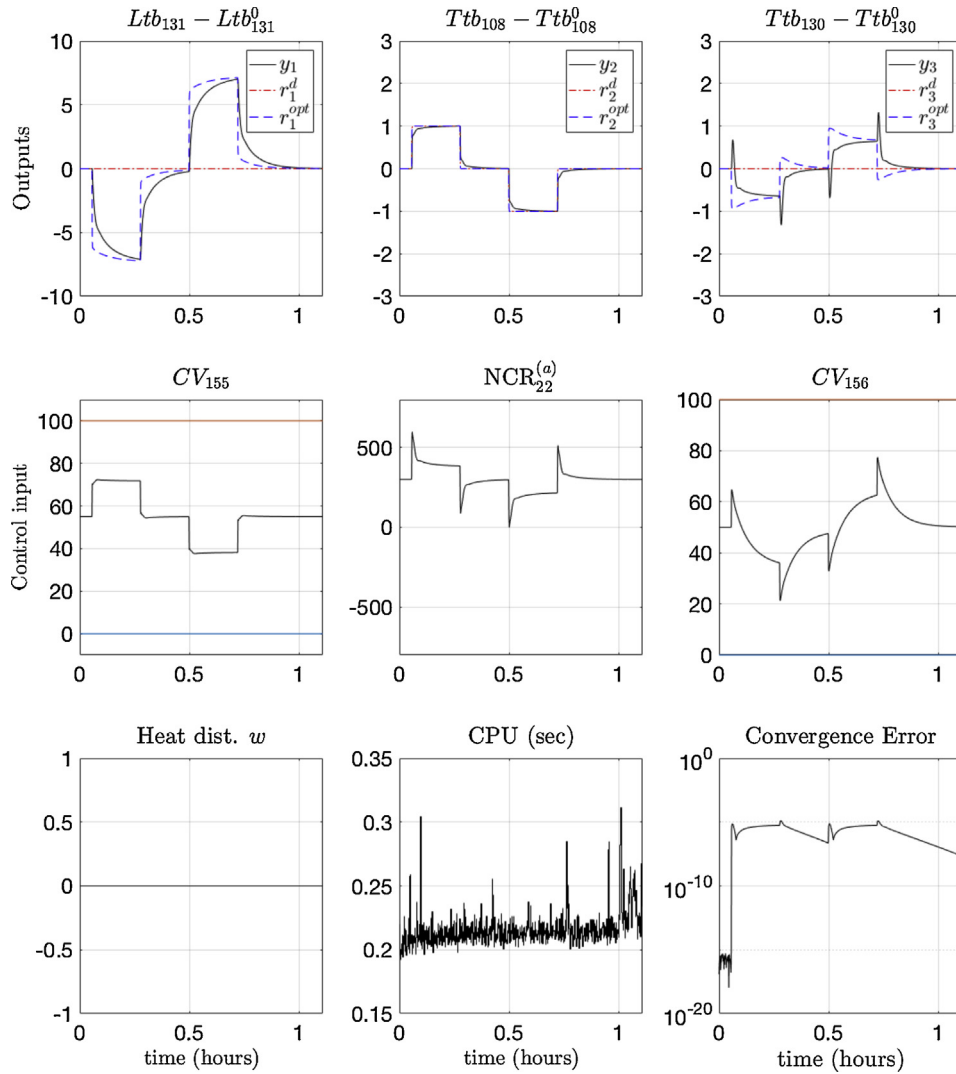


**Fig. 10.** Behavior of the closed-loop process in mode 2 in which the regulation of the variable  $Ttb_{108}$  is privileged. Note how the regulation of the helium level in the bath is softened in order to perform the required task on the regulated temperature. (For interpretation of the references to color in the text, the reader is referred to the web version of the article.)

- (3) Two typical scenarios of set-point changes on the outputs  $Ltb_{131}$  and  $Ttb_{108}$  are successively simulated under the proposed control framework.
- (4) The behavior of the fully decentralized control (assuming zero coupling signals by each local controller) is shown in order to underline the benefit from the use of the hierarchical structure.

Before addressing the issues enumerated above, some parameters that are used throughout the simulations are first described in the following section.

#### 4.1.1. The simulation parameters

The sampling time for the simulation is taken equal to  $\tau = 5$  s. This is the currently used sampling time at CEA/INAC/SBT. Moreover, it is the one that has been used in all previous studies [4,3,5]. The prediction horizon is taken equal to  $N_p\tau$  where  $N_p = 100$ . This corresponds to roughly 8 minutes. The parameter  $m = 3$  is used in the identification by the coordinator of the 10 parameters that defines quadratic cost function (42) since this choice provides  $n_r^3 = 27$  values of the cost function on a regular cloud of values of  $r$ .

The local MPC controllers are based on the local cost function (33) in which the following trivial weighting matrices are used:

$$Q_1 := 10^6 \times \mathbb{I}_{10 \times 10}; R_1 = \begin{bmatrix} 1 & 0 \\ 0 & 10 \end{bmatrix}; Q_2 = \mathbb{I}_{14 \times 14}; R_2 = 10^2 \quad (62)$$

Regarding the weighting matrices used in the central cost, the exponent  $q=20$  is used in the time-varying weighting settings; the control weighting matrices were taking systematically equal to  $R_c^{(s)} = 0$ ,  $s=1, 2$  in order to focus on the regulation performance. Regarding the output regulation weighting matrices  $Q_c^{(s)}$ , three different settings are used depending on the control mode, namely:

- (1) In the by default disturbance rejection mode, the following settings is used:

$$Q_c^{(1)} = \begin{bmatrix} 10^2 & 0 \\ 0 & 10^6 \end{bmatrix}; Q_c^{(2)} = 1 \quad (63)$$

- (2) When the second mode is activated in order to steer the level of the helium bath to some desired value, the following setting is used:

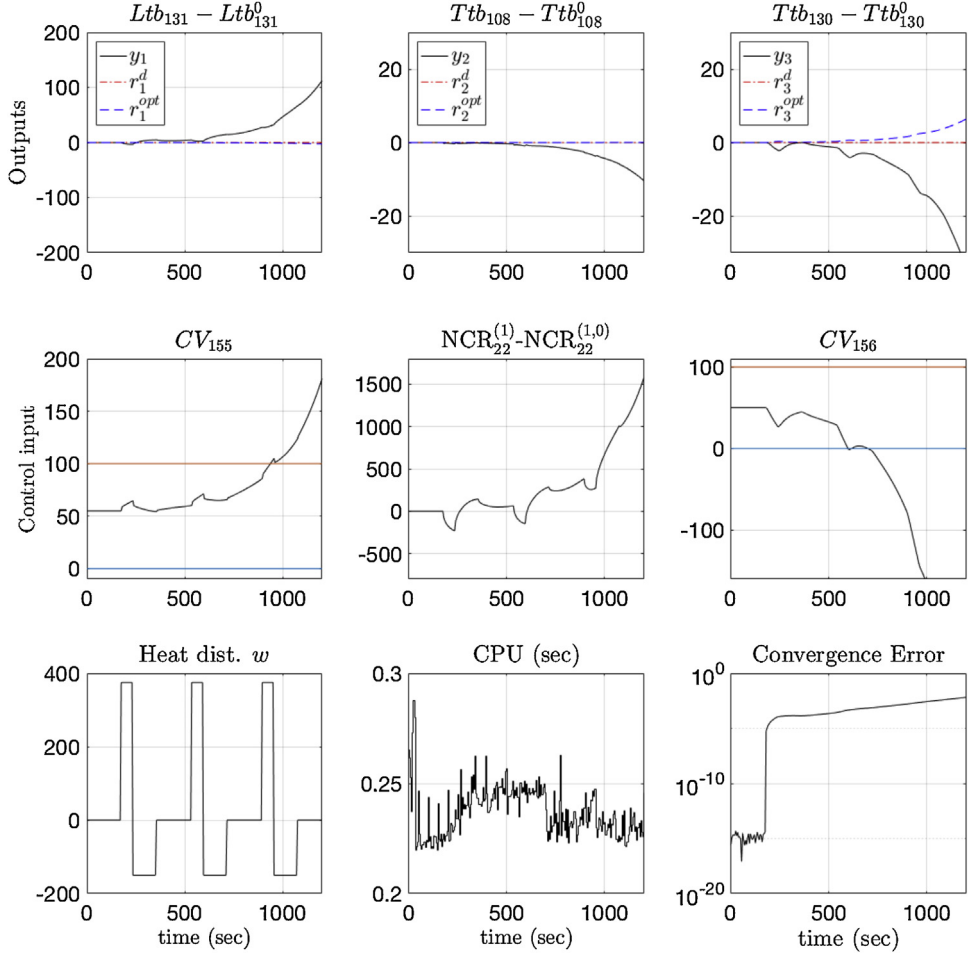


**Fig. 11.** Behavior of the **fully-decentralized** closed-loop process under the heat pulse disturbance scenario. Here, each local controller considers that there are no coupling signals (all of them set to zeros). Note that the last two plots showing the computation time and the convergence error are not relevant in this case.

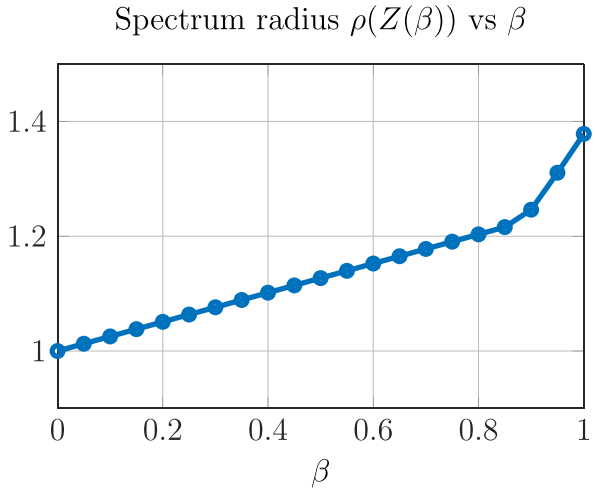


**Fig. 12.** Evolution of the spectrum of the simple filtering-based fixed point evolution matrix as a function of the filtering parameter  $\beta$  when the local MPC are defined by (66). This plot shows that the simple filtering rule cannot be used in this case and the more involved LQR-based spectrum assignment is necessary to stabilize the fixed-point iterations.

$$Q_c^{(1)} = \begin{bmatrix} 10^6 & 0 \\ 0 & 1 \end{bmatrix}; Q_c^{(2)} = 1 \quad (64)$$

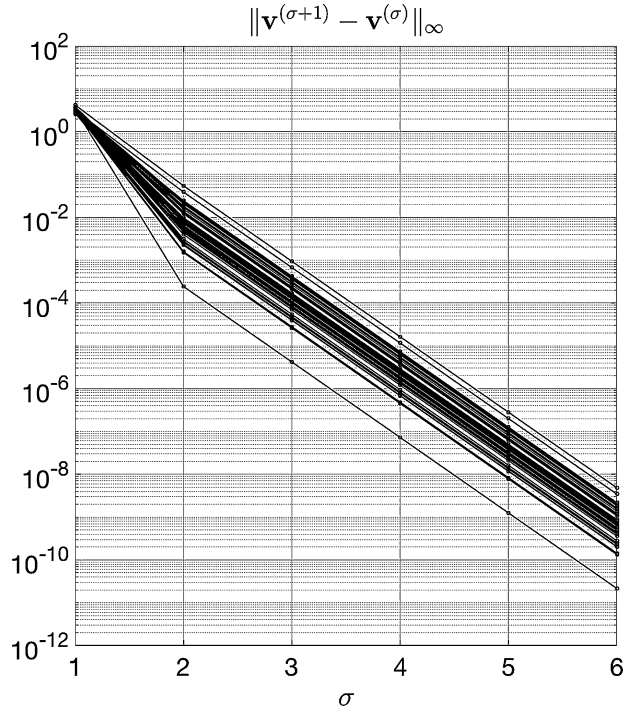


**Fig. 13.** Convergence of the fixed-point iteration for 50 random initial conditions.

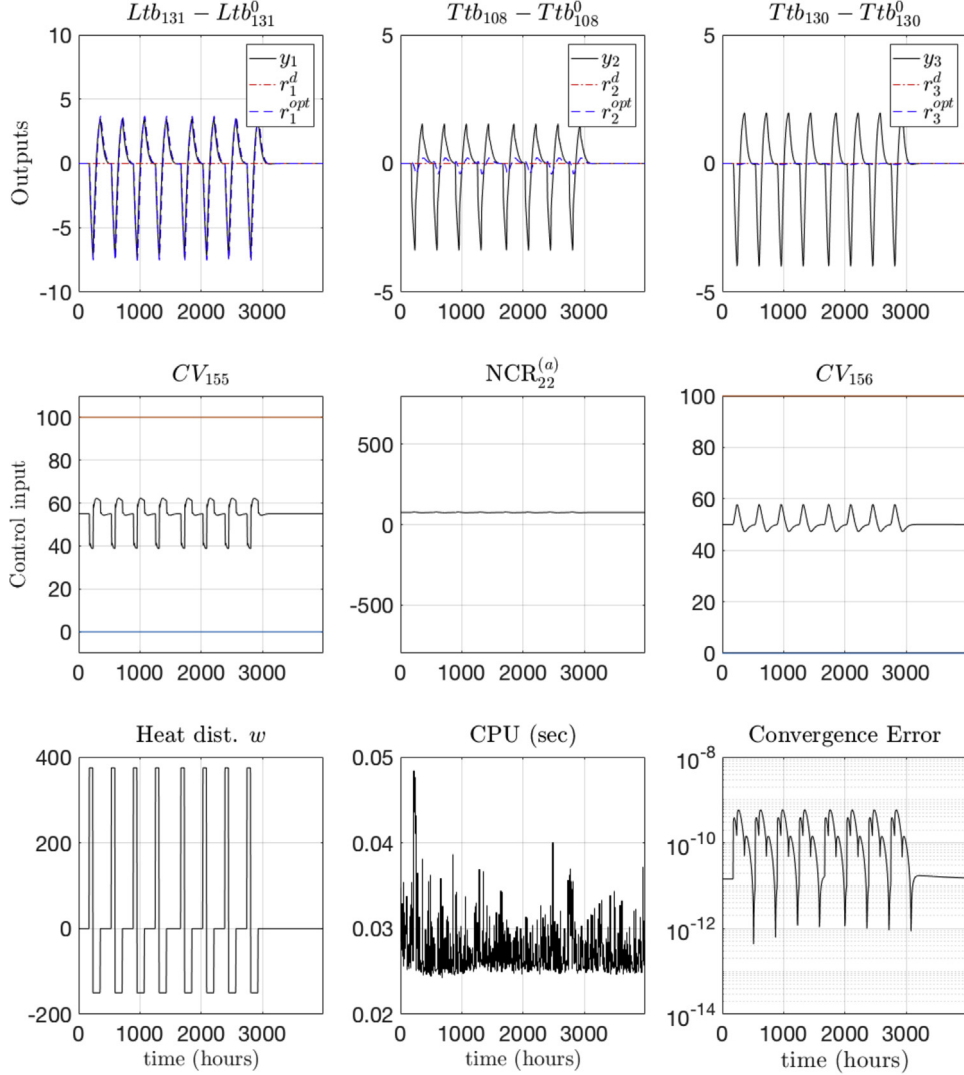


**Fig. 14.** Closed-loop behavior of the cryogenic refrigerator under the disturbance rejection mode. Note that thanks to the new setting, the control actuator \$NCR\_{22}^{(a)}\$ is almost unused. This figure is to be compared to Fig. 8. Note also the drastic reduction in the computation time that is due to the spectrum assignment enabling the convergence in much lower number of iterations.

- (3) Finally when the second mode is activated in order to steer the temperature \$Ttb\_{108}\$ to some desired value, the following settings is used:

$$Q_c^{(1)} = \begin{bmatrix} 1 & 0 \\ 0 & 10^6 \end{bmatrix}; Q_c^{(2)} = 1 \quad (65)$$

Regarding the quantities involved in the identification of the quadratic cost by the coordinator (see Section 3.2), we have \$n\_r=3\$ and \$m=3\$ and \$\Delta=1\$ are used.

#### 4.1.2. Fixed-point convergence analysis

Recall that the convergence condition (57) for the fixed point iteration does not depend on the settings of the central cost. It rather depends on the local settings and the filtering parameter \$\beta\$. Fig. 6 shows the evolution of the spectrum radius \$\rho(Z(\beta))\$ involved in the stability condition (57) as a function of the filtering coefficient \$\beta\$. This figure clearly shows that the choice \$\beta=0.5\$ is appropriate in terms of the contraction ratio.

Fig. 7 shows the evolution of the maximum error between two successive iterates during the fixed-point iterations. 50 random initial values \$\mathbf{v}^{(0)}\$ are simulated. From this figure it comes out that 400 iterations generally lead to an error less than \$10^{-5}\$ which is assumed

to be sufficiently small to stop the iterations. The fact is that a sampling period of 5 s is already largely higher than the time needed for 400 iterations (\$\approx 0.31\$ s) and hence, adopting a stopping criterion does not change the result for our application.

#### 4.1.3. Closed-loop simulations

Fig. 8 shows the behavior of the closed-loop process in response to a periodic heat pulse disturbance. This disturbance emulates the heat disturbance that comes from the experimental facilities using the cooling power to cool down the supra-conducting circuits. The level of heat pulses used in this scenario is considered to be the sizing level for the experimental cryogenic refrigerator. Note that the computation time needed for the coordinator to deliver the optimal auxiliary set-points \$r^{opt}\$ never exceed 310 ms. Moreover the convergence of the fixed-point iteration is assessed through the last plots where it can be observed that it is roughly around \$10^{-5}\$.

Fig. 9 shows the behavior of the closed-loop process when mode 2 is activated in order to steer the level of liquid in the helium bath to some desired values. Note how due to the specific settings of the weighting matrices of the central cost, the regulation of the temperature \$Ttb\_{108}\$ is softened in favor of a better regulation of

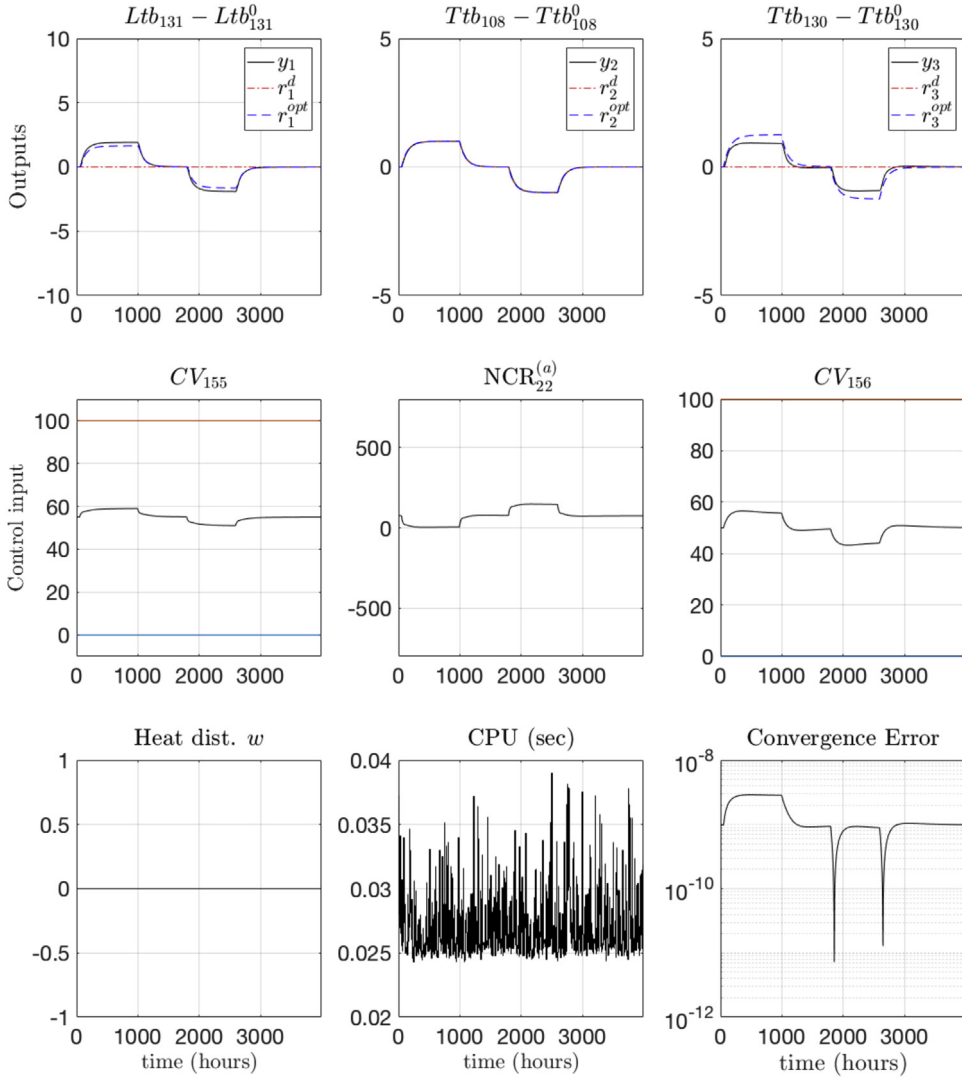


**Fig. 15.** Closed-loop behavior of the cryogenic refrigerator under the mode 2 in which a set-point change on  $Ttb_{108}$  is applied. This figure is to be compared to Fig. 9. Note also the drastic reduction in the computation time that is due to the spectrum assignment enabling the convergence in much lower number of iterations.

the level. This can be shown by examining the difference between the central desired values  $r^d$  (in axis-like red lines on the plots) and the auxiliary set-points  $r^{opt}$  (in dashed blue lines on the plots).

Fig. 10 shows the behavior of the closed-loop process when mode 2 is activated in order to steer the temperature  $Ttb_{108}$  of the JT valve to some desired values. Note how due to the specific settings of the weighting matrices of the central cost in this case, the regulation of the level  $Ltb_{131}$  in the helium bath of subsystem  $S_1$  is softened in favor of better regulation of the JT temperature. This can be shown by examining the difference between the central desired values  $r^d$  (in axis-like red lines on the plots) and the auxiliary set-points  $r^{opt}$  (in dashed blue lines on the plots).

It is worth underlying that the number of iterations (=400) is probably over pessimistic and a precision of  $10^{-5}$  on the fixed-point iteration error is not necessary. Simulations proving this fact are not produced here as the plots are roughly the same as the ones presented. This means that the computation time can be divided by 2 without noticeable performance losses.

Finally, Fig. 11 shows the behavior of the **fully decentralized** controller, namely, when each local controller considers that the coupling signal is vanishing. This scenario underlines the destabilizing character of the coupling signals involved in the cryogenic

refrigerator. It is worth emphasizing that in this context, the last two plots (cpu time and convergence error) are not relevant.

Although the previous results support the claim that the problem is theoretically solved, it remains true that the use of the control input  $NCR_{22}^{(a)}$  is such that a steady heating power of roughly  $NC_{22}^{(a,0)} = 350$  W is necessary to make the resulting control feasible. These 350 W are therefore removed from the amount of useful heating power that can be managed by the cryogenic refrigerator. Attempts to reduce the use of this actuator by increasing its penalty in the local MPC design leads to a reduction of the authority of the control in the local MPC design of subsystem  $S_1$  and this induces an unstable closed-loop system. Even when some parameter tuning choices are successful in terms of local closed loop stability, it came out that the simple filtering rule cannot enforce the convergence of the fixed-point iteration.

In the next section, it is shown that the combination of the non-conventional time varying penalties in the local MPC together with the spectrum assignment of the fixed-point iteration map through LQR design can successfully address the problem. Indeed, the non-conventional definition of the cost function through time varying penalty enforces the stability of the local MPC closed-loop and the convergence of the resulting fixed-point iteration is enforced by the spectrum assignment.

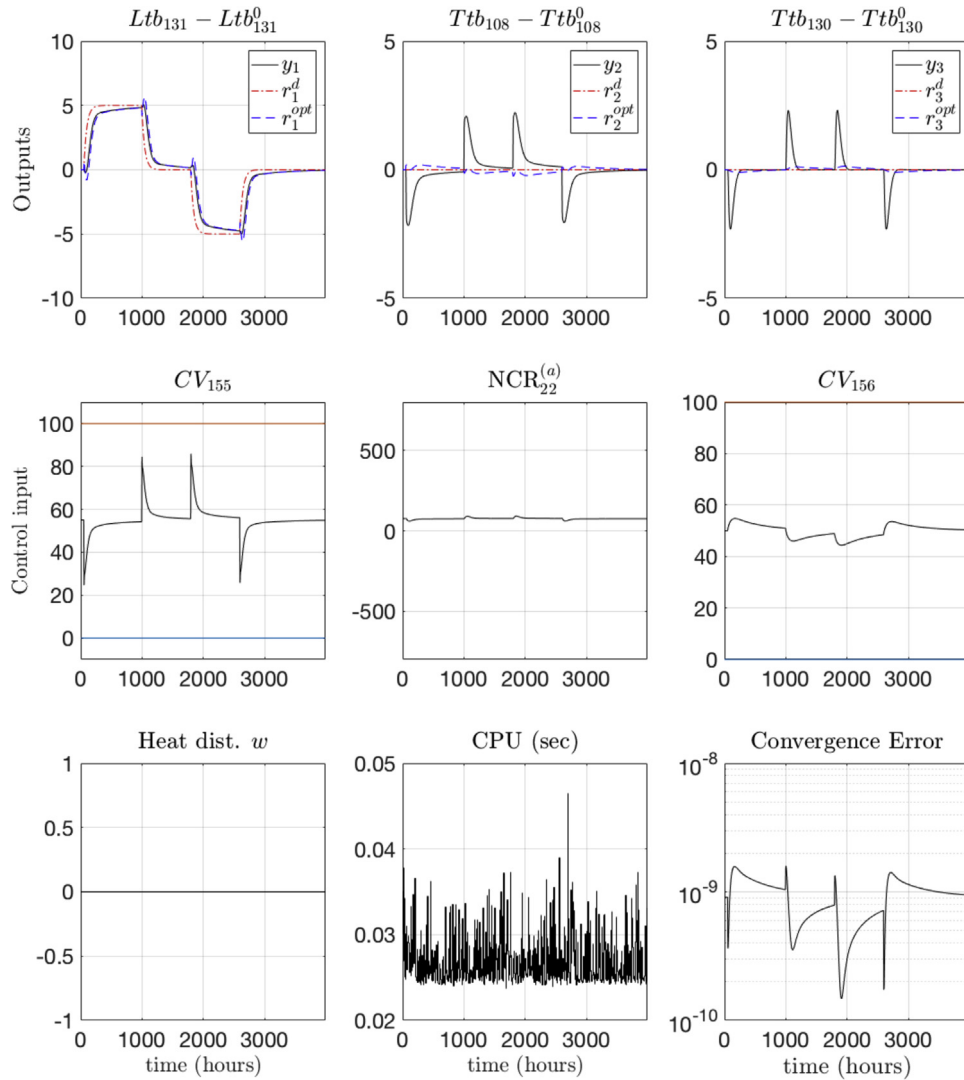


**Fig. 16.** Closed-loop behavior of the cryogenic refrigerator under the mode 2 in which a set-point change on Ltb<sub>131</sub> is applied. This figure is to be compared to Fig. 10. Note also the drastic reduction in the computation time that is due to the spectrum assignment enabling the convergence in much lower number of iterations.

#### 4.2. Results with time varying weighting and spectrum assignment via LQR design of the fixed-point iteration filter

Based on the discussion above, a new tuning is obtained that focuses on reducing the use of the control input NCR<sub>22</sub><sup>(a)</sup>. The following design is obtained for the local MPCs:

$$Q_1 := \mathbb{I}_{10 \times 10}; R_1 = 10^{-3} \mathbb{I}_{2 \times 2}; Q_2 = \mathbb{I}_{14 \times 14}; R_2 = 10^3 \quad (66)$$

Moreover, the exponents  $q_1 = 4$  and  $q_2 = 3$  are now used in the definition of the cost functions used in the local MPC design [see (33)]. This enables a drastic reduction in the prediction horizon length since  $N_p = 25$  is now compatible with the stability requirement. This reduction in  $N_p$  enables the computation time to be reduced as it is shown in the CPU-time so obtained.

Note that in this setting, the exponent  $q$  used in the central cost (21) is now set to 0 while the following weighting matrices settings are used in the definition of the central cost, depending on the regulation/disturbance rejection mode being addressed<sup>9</sup>:

- (1) In the by default disturbance rejection mode, the following settings is used:

$$Q_c^{(1)} = \begin{bmatrix} 10^{-2} & 0 \\ 0 & 10^3 \end{bmatrix}; Q_c^{(2)} = 5; R_c^{(1)} = \begin{bmatrix} 10^{-3} & 0 \\ 0 & 10 \end{bmatrix}; R_c^{(2)} = 10^{-3} \quad (67)$$

- (2) When the second mode is activated in order to steer the level of the helium bath to some desired value, the following setting is used:

$$Q_c^{(1)} = \begin{bmatrix} 10^3 & 0 \\ 0 & 1 \end{bmatrix}; Q_c^{(2)} = 10^{-3}; R_c^{(1)} = \begin{bmatrix} 10^{-3} & 0 \\ 0 & 10 \end{bmatrix}; R_c^{(2)} = 10^{-5} \quad (68)$$

- (3) Finally when the second mode is activated in order to steer the temperature Ttb<sub>108</sub> to some desired value, the following

<sup>9</sup> Note that only the weighting matrices for the central cost are changed while the local MPC keep the same setting defined by (66).

settings is used:

$$Q_c^{(1)} = \begin{bmatrix} 10^{-5} & 0 \\ 0 & 10^5 \end{bmatrix}; Q_c^{(2)} = 2 \times 10^{-3}; R_c^{(1)} = \begin{bmatrix} 10^{-7} & 0 \\ 0 & 10^{-2} \end{bmatrix}; R_c^{(2)} = 10^{-6} \quad (69)$$

**Fig. 12** shows that with the local MPC setting defined by (66), there is no appropriate values of the simple filtering parameter  $\beta \in [0, 1]$  that lead to a convergent fixed-point iteration. Therefore, a LQR-based filtering design is necessary here.

**Fig. 13** shows the convergence of the fixed-point iterates for 50 randomly generated initial conditions. Note the reduced number of needed iterations before reaching convergence that can be assigned to the fixed-point iteration through the LQR design of the updating matrix. The design is done here using the state weighting matrix  $10^6 \times \mathbb{I}$  and the control weighting matrix  $10^{-4} \times \mathbb{I}$  in the LQR design.

**Figs. 14–16** show the closed-loop behavior of the cryogenic refrigerator under the hierarchical control using the setting defined by (66)–(69) together with the fixed-point iteration matrix defined through the LQR design explained at the end of Section 3.3.

These figures clearly show that the new setting parameter enables a drastic reduction in the steady value of the control-related heating power which can be decreased from  $NC_{22}^{(a,0)} = 350\text{W}$  to 75 W. Moreover, this last value is made necessary only when set-point change in the regulated variable  $Ttb_{108}$  is required. This can be set specifically in this case since it occurs only in a specific operation during which the refrigerator is not faced with heat pulse disturbances. However, if one only focuses on the disturbance rejection scenario depicted in **Fig. 14**, it can be observed that a value as low as  $NCR_{22}^{a,0} = 5\text{W}$  can be sufficient to reject the disturbance using the controlled valves with very small participation of the control input  $NCR_{22}^a$ .

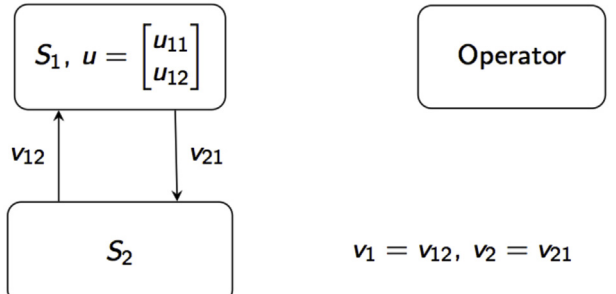
Another important feature can be observed regarding the computation time where the combined effects of reducing the prediction horizon length to  $N_p = 25$  rather than  $N_p = 100$  and the much fewer number of iterations required before tight convergence through the spectrum assignment of the fixed-point iteration enable to reduce the computation time by an order of magnitude (decreasing it from 300 ms to 40 ms). This is a crucial issue as the PLC used on the cryogenic refrigerator is far more slower than a desk computer on which the computation times are systematically evaluated. The current figures enable an industrial PLC up to 100 times slower than the desk computer used to produce the simulation results to be used in order to implement the proposed scheme.

## 5. Further discussion: handling operator handover

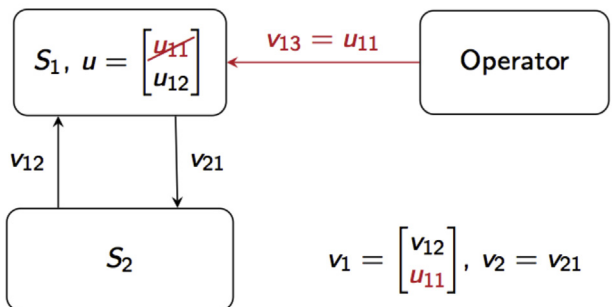
In industrial context, it is mandatory that the control architecture allows operator handover on the controlled process. These are predefined modes where the operator informs the control system that he (she) wishes to partially short-circuit the control logic in order to directly deliver his (her) own decision.

Depending on the level of the decision the operator wishes to deliver, two handover levels can be defined:

- (1) In the first, the operator decides to deliver one (or more) auxiliary set-point, say  $r_j$  instead of this set-point being computed by the coordinator of the hierarchical architecture. Handling this case is extremely easy as all the coordinator needs to do is to



(a) Before operator handover on  $u_{11}$



(b) After operator handover on  $u_{11}$

**Fig. 17.** Schematic view of the way low level operator handover can be handled.

replace the unconstrained expression (46) of the optimal  $r^{opt}$  by the constrained one given by:

$$r^{opt}(k) = \underset{r}{\operatorname{argmin}} \hat{J}(r) \text{underr}_j = r_j^{operator} \quad (70)$$

Nothing else has to be changed in the control architecture as explained in the previous sections.

- (2) In the second level, the operator decides to take the direct control of some actuator value, say the first control input  $u_{11}$  of subsystem  $S_1$  (see **Fig. 17**). Assume that before this decision the coupling signals between subsystems  $S_1$  and  $S_2$  were given by (see **Fig. 17**):

$$v_1 = v_{12}; v_2 = v_{21} \quad (71)$$

Now when the operator decides to be directly involved, it comes obviously that the operator should be viewed as an additional new subsystem, say  $S_3$  which acts on subsystem  $S_1$  through the signal  $u_{11}$ .<sup>10</sup> Therefore, the operator handover at this level can be handled by two changes (see **Fig. 17(b)**):

- (a) First the subsystem  $S_1$  loses the control input  $u_{11}$ ,
- (b)  $u_{11}$  is transformed into a new component of the coupling signal  $v_1$ , that is:

$$v_1 = \begin{bmatrix} v_{12} \\ u_{11} \end{bmatrix}; v_2 = v_{21} \quad (72)$$

Now this change sets obviously a new hierarchical framework that needs to be assessed and tuned using the same tools and concepts described above. In particular, it can be revealed that for some handover modes, the stability of the system might be threatened

<sup>10</sup> Another way to view the situation is to consider that the operator is embedded inside subsystem  $S_2$  which now acts on subsystem  $S_1$  from which the control input has been removed.

and/or the tuning of the filtering and the local weights need to be different. The contribution of this paper gives the theoretical background to rationally address this crucial industrial question.

## 6. Conclusion and further investigations

In this paper, a complete framework is proposed for the design of a hierarchical control structure that addresses the issues of modularity, privacy and distributed computation that arise in the industrial process control context. The framework is presented in the case where MPC control design is used in the local level. However, it goes without saying that the same framework can be used in the more common case where local PID controllers are used at the local level. Indeed, when PID controllers (or any other linear controllers) are used in the local level, the subsystems can still send the predictions of their coupling signals if the exogenous signals acting on them are given by the coordinator. This enables the convergence of the fixed-point iteration to be studied and the appropriate tuning changes to be undertaken if necessary. This enables the use of the proposed scheme in coordinating the overall consequences of the network of local controllers.

Natural extension of the present work concerns constraints handling as well as experimental validation on the real process. Using the available nonlinear knowledge-based model is also under investigation.

## References

- [1] M. Alimir, Stability proof for nonlinear MPC design using monotonically increasing weighting profiles without terminal constraints, *Automatica* (2017) (accepted). arXiv:1703.02761.
- [2] D. Barcelli, A. Bemporad, G. Ripaccioli, Hierarchical multi-rate control design for constrained linear systems, in: Proceedings of the 49th IEEE Conference on Decision and Control, Atlanta, GA, USA, 2010, pp. 5216–5221.
- [3] F. Bonne, M. Alimir, P. Bonnay, Nonlinear observers of the thermal loads applied to the helium bath of a cryogenic Joule–Thomson cycle, *J. Process Control* 24 (3) (2014) 73–80.
- [4] F. Bonne, M. Alimir, P. Bonnay, B. Bradu, Model based multivariable controller for large scale compression stations. design and experimental validation on the LHC 18 kW cryorefrigerator, in: Proceedings of the Cryogenic Engineering Conference CEC, Anchorage, AK, USA, 2013.
- [5] F. Bonne, M. Alimir, Ch. Hoa, P. Bonnay, M. Bon-Maridou, L. Monteiro, A simulink library for cryogenic components to automatically generate controls schemes for large cryorefrigerators, *IOP Conf. Ser. Mater. Sci. Eng.* 101 (1) (2015).
- [6] François Bonne, Mazen Alimir, Patrick Bonnay, Experimental investigation of control updating period monitoring in industrial PLC-based fast MPC: application to the constrained control of a cryogenic refrigerator, *Control Theory Technol.* 15 (2) (2017) 92–108.
- [7] M.D. Doan, T. Keviczky, B. De Schutter, A distributed optimization approach for hierarchical MPC of large-scale systems with coupled dynamics and constraints, in: Proceedings of the 50th IEEE Conference on Decision and Control, Orlando, FL, USA, 2011.
- [8] M.D. Doan, T. Keviczky, B. De Schutter, A hierarchical MPC approach with guaranteed feasibility for dynamically coupled linear systems, in: R.R. Negenborn, J.M. Maestre (Eds.), *Distributed Model Predictive Control Made Easy*, Volume 69 of *Intelligent Systems, Control and Automation: Science and Engineering*, Springer, Dordrecht, The Netherlands, 2014, pp. 393–406.
- [9] P. Bonnay, A. Barraud, G. Bornard, F. Clavel, M. Alimir, C. Deschildre, Multivariable control architecture for a cryogenic test facility under high pulsed loads: model derivation, control design and experimental validation, *J. Process Control* 21 (7) (2011) 1030–1039.
- [10] D.Q. Mayne, J.B. Rawlings, C.V. Rao, P.O.M. Scokaert, Constrained model predictive control: stability and optimality, *Automatica* 36 (2000) 789–814.
- [11] R.R. Negenborn, J.M. Maestre, On 35 Approaches for Distributed MPC Made Easy, Springer, Dordrecht, Netherlands, 2014, pp. 1–37.
- [12] C. Ocampo-Martinez, D. Barcelli, V. Puig, A. Bemporad, Hierarchical and decentralized model predictive control of drinking water networks: application to Barcelona case study, *IET Control Theory Appl.* 6 (1 (January)) (2012) 62–71.
- [13] B. Picasso, D. De Vito, R. Scattolini, P. Colaneri, An MPC approach to the design of two-layer hierarchical control systems, *Automatica* 46 (2010) 823–831.
- [14] J.B. Rawlings, D. Angeli, C.N. Bates, Fundamentals of economic model predictive control, in: 2012 IEEE 51st IEEE Conference on Decision and Control (CDC), 2012, December, pp. 3851–3861.
- [15] P. Roussel, A. Girard, B. Jager, B. Rousset, P. Bonnay, F. Millet, P. Gully, The 400 W at 1.8 K test facility at CEA Grenoble, *AIP Conf. Proc.* 823 (1) (2006) 1420–1427.
- [16] R. Scattolini, Architectures for distributed and hierarchical model predictive control – a review, *J. Process Control* 19 (2009) 723–731.
- [17] B.T. Stewart, J.B. Rawlings, S.J. Wright, Hierarchical cooperative distributed model predictive control, in: Proceedings of the American Control Conference, Baltimore, MD, USA, 2010.